A Proposal for a Parameterized Circulating Vector Field Guidance for Fixed Wing Unmanned Aerial Vehicles

A thesis presented to

the faculty of

the Russ College of Engineering and Technology of Ohio University

In partial fulfillment

of the requirements for the degree

Master of Science

Garrett S. Clem

May 2018

This thesis titled

A Proposal for a Parameterized Circulating Vector Field Guidance for Fixed Wing Unmanned Aerial Vehicles

by

GARRETT S. CLEM

has been approved for

the Department of Mechanical Engineering

and the Russ College of Engineering and Technology by

Jay P. Wilhelm

Assistant Professor of Mechanical Engineering

Dennis Irwin

Dean, Russ College of Engineering and Technology

Abstract

CLEM, GARRETT S., M.S., May 2018, Mechanical Engineering

A Proposal for a Parameterized Circulating Vector Field Guidance for Fixed Wing Unmanned Aerial Vehicles (62 pp.)

Director of Thesis: Jay P. Wilhelm

Unmanned Aerial Vehicles (UAVs) are guided to fly along straight line obstacle free paths that connect pre-planned waypoints. Initially undiscovered obstacles encountered during flight may require waypoints to be re-planned. Obstacles could be avoided without the need to re-plan mission waypoints by implementing vector field path following in conjunction with repulsive obstacle vector fields. Repulsive vector fields that combine weighted repulsive and attractive components to provide an optimal obstacle avoidance guidance will be investigated to avoid singularities and improve path tracking performance compared to waypoint guidance.

Table of Contents

List of Figures

List of Symbols

$\vec{v}$	Vector field
$\vec{v}_{conv}$	Convergence component
$\vec{v}_{circ}$	Circulation component
$\vec{v}_{tv}$	Time-varying component
G	Convergence weight
H	Circulation weight
L	Time-varying weight
q	Spatial dimension set
$\alpha_i(x_1, x_2, ...x_n, t)$	Implicit surface function
n	Number of spatial dimensions
t	Time
i	index
∇_q	Gradient with respect to spatial dimensions q
M	Gradient matrix
a	Velocity column vector
$\vec{V}$	Total field
d	Range
P	Decay weight
R	Radius
$\vec{v}_{repulsive}$	Repulsive vector field
$\vec{v}_{attractive}$	Attractive vector field
u	Speed

List of Acronyms

UAV	Unmanned Aerial Vehicles
VF	Vector Field
UAS	Unmanned Aerial System
VFF	Virtual Force Field
TPLVF	Tangent Plus Lyapunov Vector Field
RRT*	Optimal Rapid Radom Trees
DT	Delauny Triangulation
GVF	Gradient Vector Field

1 INTRODUCTION

1.1 Motivation and Problem Statement

Fixed wing Unmanned Aerial Vehicles (UAVs) are used for missions such as surveillance and reconnaissance that might put pilots in harm's way [1]. Missions typically consist of sequential objectives represented as waypoints that the UAV follows. Waypoints may be pre-planned before flight where vehicle constraints and obstacles can be considered to prevent collisions or entry into no-fly zones. UAVs follow waypoints by implementing guidance algorithms that calculate headings to direct a UAV along a path connecting the waypoints. Obstacles may be discovered during flight that were unknown at initial planning and a new set of waypoints may have to be generated. Waypoints are typically computed at a ground station and are relayed to the UAV by radio, which may be problematic if communication with the UAV is lost. Guidance that accomplishes mission objectives while avoiding obstacles without the need for re-planning waypoints may be beneficial.

Vector Field (VF) guidance is a method that is mainly used for path following and can be useful for obstacle avoidance [**?**, 2]. VFs can produce continuous heading vectors that can be used to guide a UAV to coverage and follow a path. Vectors are calculated by summing together convergence and circulation terms that are weighted by static scalars. Obstacles can be represented as a path and given a negative convergence weight resulting in a repulsive field. Static repulsive VFs do not always route the UAV around an obstacle. Modifying repulsive VF parameters to be functions of common UAV states may be used to produce an optimal guidance. **The proposed research seeks to determine VF weighting functions that enable optimal obstacle avoidance.**

1.2 Methods Overview

The proposed research was conducted in three phases consisting of numerical simulations and indoor flight experiments. Phase I consisted of demonstrating and numerically locating VF guidance singularities in a summed vector field. Static repulsive field weights and decay radius were investigated and optimized to produce minimal path deviation using VF guidance in simulation in Phase II. Lastly, flight experiments using a indoor flying quadcopter using the optimized VF guidance under fixed-wing UAV constraints was conducted.

1.3 Phase I

Characterize and present a method for locating singularities in a summed GVF. A simulation environment will be built that generates GVFs consisting of mission paths and obstacles. Circular obstacles will be investigated and the resulting singularities will be characterized. Static weights will be used and the performance of the guidance measured in distance traveled and time of flight.

1.4 Phase II

Determine combination of GVF circulation and decay radius for least cost circular obstacle avoidance. UAV closing rate, position, and range will be used to develop dynamic GVF weights for convergence and circulation. The modified GVF will be compared against a static and strictly repulsive GVF. Distance traveled and time of flight will be used to as metrics to compare the modified GVF to the unmodified GVF.

1.5 Phase III

Demonstrate optimized GVF guidance on multirotor UAV flying with fixed wing turn-rate constraints. The modified GVF developed in Phase II will be implemented

on a differential multirotor UAV emulating a fixed wing UAV Dubins constraints. Guidance performance while avoiding static circular obstacles will be demonstrated.

1.6 Summary of Objectives

Each phase consists of an **objective** that was accomplished by executing several *tasks*. Completion of all objectives and phases will result in the final deliverable.

Phase I Objective: Demonstrate and locate singularities in a summed gradient vector field
Tasks:

1. *Build a GVF simulation environment*
2. *Evaluate scenarios where singularities are expected*
3. *Characterize location of singularities*

Phase II Objective: Determine combination of repulsive gradient vector field circulation and decay radius that minimizes path deviation
Tasks:

1. *Formulate circulation and convergence weights as functions of UAV state*
2. *Determine combination of GVF weights that produces optimal guidance in simulation*

Phase III Objective: Validate modified gradient vector field guidance with indoor quadrotor experiments
Tasks:

1. *Build differential drive robot*
2. *Build robotic framework to take guidance commands*

3. *Repeat simulations performed in Phase II on ground robot*

Deliverable: Adaptive GVF parameterized weights optimal guidance for path following and static obstacle avoidance.

2 Literature Review

2.1 Literature Review Introduction

2.2 Unmanned Aerial Vehicles

Unmanned aerial vehicles (UAVs) are gaining popularity in military and civilian communities for their ability to autonomously perform tasks such as data collection, target tracking, and package delivery. In general, UAVs are categorized into fixed wing and rotor craft varieties [8] that range in size, payload, and flight time capabilities. Fixed wing UAVs (Figure 2.1a) are typically used for tasks that require larger payloads, such as cameras and cargo, and longer flight times. Multirotor UAVs (Figure 2.1b), in general, have lower payload capabilities compared to fixed wing UAVs, however do not require a large clearing for takeoff and landing and have a small turning radius making them more maneuverable.

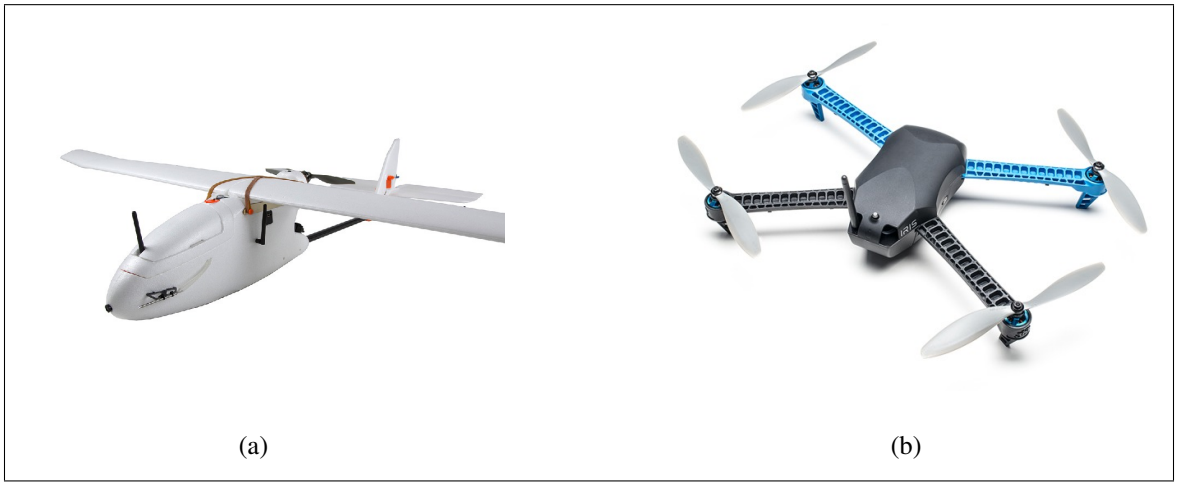

(a) (b)

Figure 2.1: Fixed wing (a) and multirotor (b) UAVs

Using UAVs has several advantages over manned aircraft consisting of low operating cost, reduced risk to human operators, and the ability to perform mundane and repetitive tasks autonomously without heavy human interaction. Open source and versatile autopilots developed by a world-wide community of hobbyist and professionals have made

UAV technology widely available on relatively inexpensive hardware [pixhawk, ardupilot]. UAVs can be piloted remotely, removing pilots from potentially dangerous situations if an aircraft experiences mechanical failure. The power behind UAVs lies in their ability to be programmed to carry out tasks autonomously and with little human interaction, allowing operators to monitor multiple vehicles simultaneously. Tasks may be carried out by a single UAV or in cooperation other air or ground vehicles [5–7]. The aircraft's route can be controlled directly by an operator's radio controller input when the vehicle is within line-of-sight (LOS). For long endurance or beyond LOS missions, the UAV can be programmed to autonomously follow a mission path that is typically generated prior to flight on a dedicated ground station. Flying autonomous missions typically requires not only the UAV and the autopilot, but a ground support station and hardware to communicate with the ground.

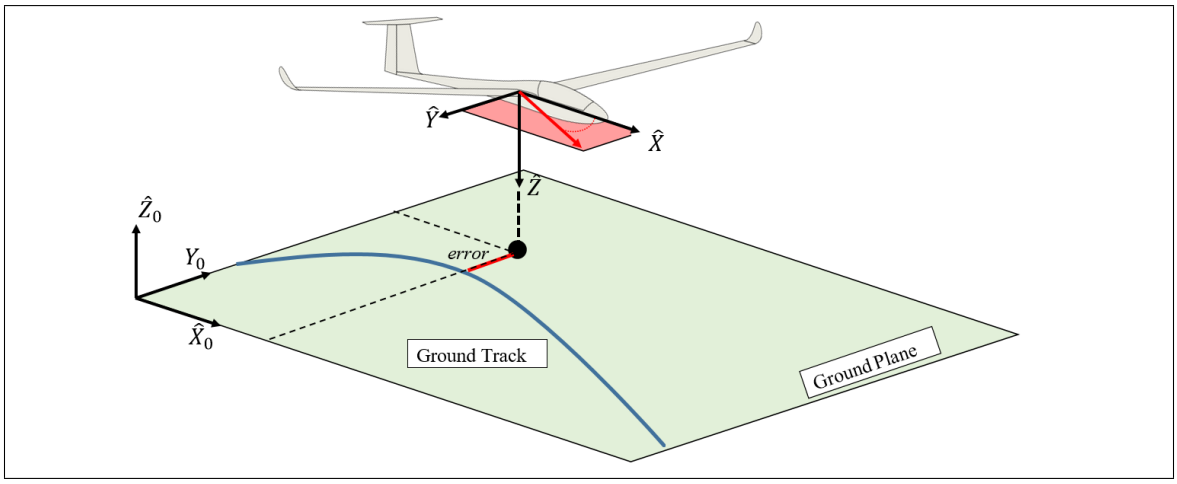

Figure 2.2:

2.3 Unmanned Aerial Systems (UAS)

These UAVs and autopilots are part of an Unmanned Aerial System (UAS) which work in conjunction with ground stations, radio control transmitters, and two way radios. The UAV craft provides the support structure, lifting and control surfaces, and housing for the autopilot, radios, and sensors. Ground stations are responsible for monitoring the

vehicle's status, planning missions, and generating obstacle free and flyable paths which are sent to the autopilot via two way radio.

2.3.1 Ground Stations

Ground stations are the hardware and software framework used to configure UAV settings, plan missions, and collect mission data. Commercial open source ground stations such as qground control depend on a human operator's knowledge of the environment to plan an obstacle free path. Takeoff, landing, and emergency return-to-home locations are designated in safe clearings capable of accommodating the vehicle. Other tasks such as area surveying and loitering can be assigned at certain points along the mission path. An example of a mission consisting of taking off, surveying, and landing is shown in Figure 2.3

Figure 2.3: Ground station software planning a waypoint based mission

Mission paths are typically represented as a series of finite waypoints that are relayed to the UAV over radio where an on-board guidance system interprets them.

==========

Obstacle free and flyable paths are typically pre-planned and generated off-line at a dedicated ground station using a path planner. Many methods can be used for generating paths, however the process is generally executed in two steps consisting of optimization and refinement. Optimization builds shortest path taking in constraints such as obstacles and mission objectives. The optimized path is then refined to meet a vehicles dynamic constraints, such as turn rate and velocity.

==========

2.3.2 Autopilot

The UAV autopilot is responsible for controlling a pre-planned path and maintaining vehicle stability while under the influence of external wind disturbances. Stable flight while path following is accomplished by implementing feed-back control, navigation, and guidance systems. A high level overview of the autopilots systems can be seen in Figure 2.4. Feed-back refers to the closure of an open-loop control system which allows a reference error to be calculated between the desired state of the UAV, the reference, and the current state of the UAV. Reference error is used to calculate the necessary actuator output required to modify the vehicles attitude and position while preventing unbounded oscillation. Attitude and position feed-back is provided by the navigation system by sampling on-board sensors such as global position system (GPS) and inertial measurement units (IMUs). Filtering and fusing noisy data from multiple sources is often accomplished through estimation techniques such as the Kalman filter.

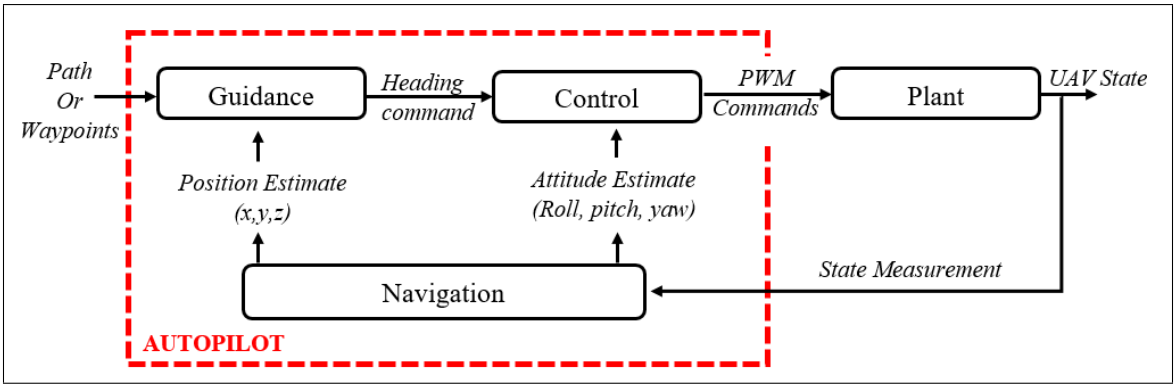

Figure 2.4: Autopilot's Navigation, Guidance, and Control Architecture

2.4 UAV Guidance

On-board guidance systems attempt to minimize the lateral error to the path by commanding a heading pointing to the path. Guidance methods for following a pre-planned path include geometric methods such as waypoint or carrot chasing and control techniques such as proportional-integral-derivative (PID), non-linear guidance laws, and linear quadratic regulator (LQR) [9]. Due to traditional guidance method's dependence on a path planner to construct an obstacle free and flyable path, these methods often lack a mechanism to avoid new obstacles. Re-planning and relaying a new obstacle free path may be impossible under certain conditions, such as flying beyond line-of-sight. Path planning on-board to avoid a new obstacle could be accomplished by inserting a new temporary path or by completely re-planning, however introduces several challenges such as waypoint placement and density. It would be beneficial to include obstacle avoidance into a UAVs guidance system to remove the need to communicate with the ground station or use an on-board path planner which may be accomplished with potential field or vector field.

2.4.1 Potential Field

Potential field is based on the principle of artificial attractive and repulsive forces acting on a point mass that is guided to a desired goal while avoiding static and dynamic

obstacles [10]. Goal states are represented as an attractive force that pulls a point mass in the direction of minimal energy while obstacles are represented as repulsive forces that act locally to push the point mass away. Potential field is also capable of acting as a path and trajectory planning algorithm [11], possibly eliminating the off-board path planner.

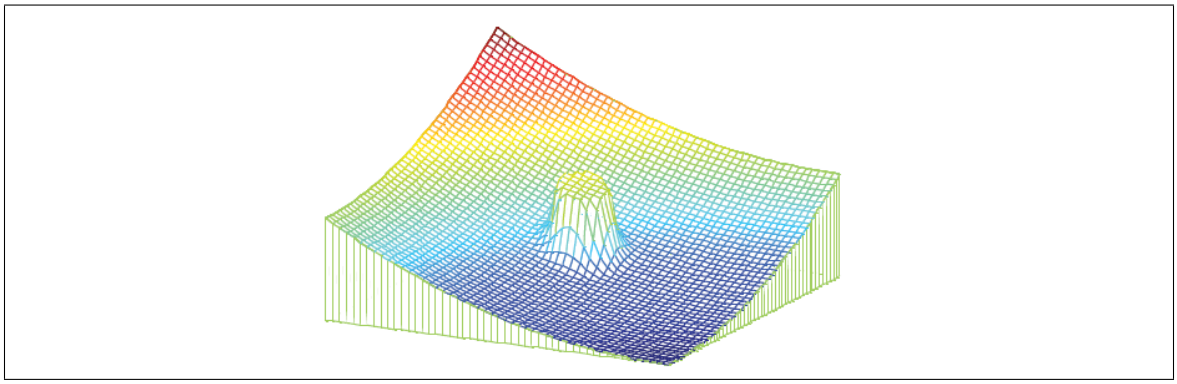

Figure 2.5: Single Obstacle Potential Field Gradient [12]

An example of potential field can be found in [13–15] which allowed for real time goal seeking with obstacle avoidance on a mobile ground robot equipped with ultrasonic sensors. The robot located at (x_0, y_0) is attracted towards a goal with constant magnitude force $\overrightarrow{F_t}$ located at (x_t, y_t) and a distance d_t from the robot. In the immediate area of the robot, an active window exists which records integer certainty values inside discrete cells. Cells containing an obstacle provide a repulsive force $\overrightarrow{F_{i,j}}$ opposite in direction to the line-of-sight from vehicle to cell location (x_i, y_j), where (i, j) represents the cell index, F_{cr} is a constant repulsive force, W the vehicle's width, $C_{i,j}$ a cell's certainty, and $d_{i,j}$ the distance to the center of the cell with respect to robots center.

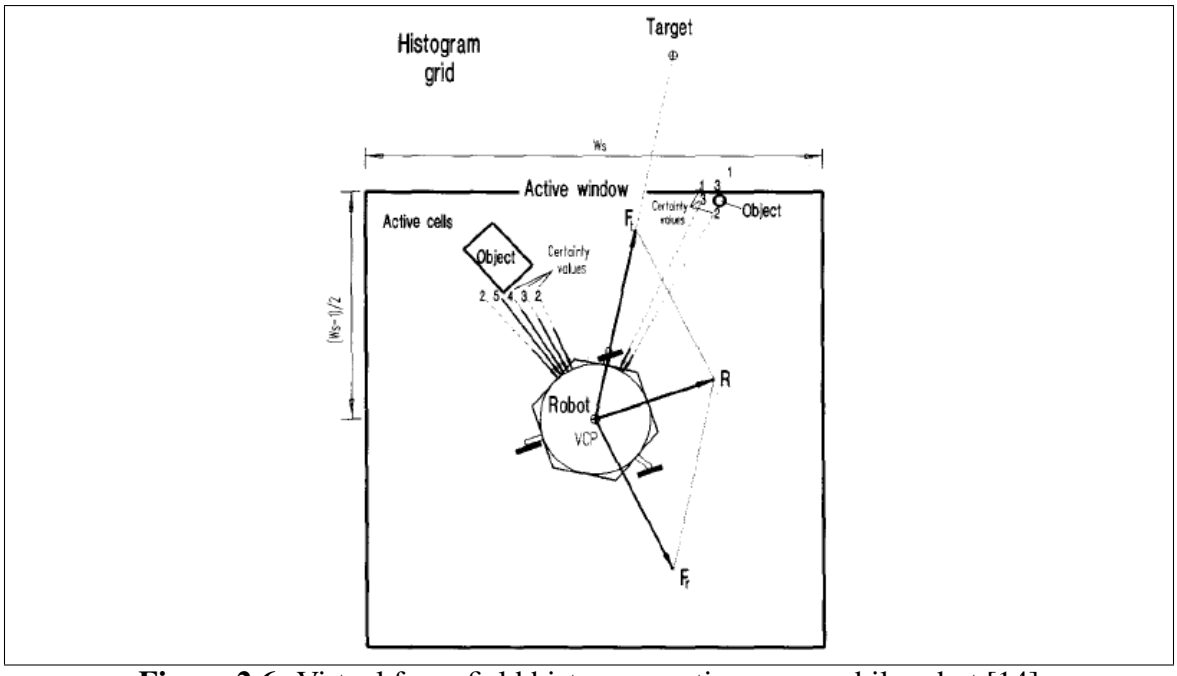

Figure 2.6: Virtual force field histogram acting on a mobile robot [14]

$$\overrightarrow{F_{i,j}} = \frac{F_{cr} W^n C_{i,j}}{d_{i,j}^n}\left(\frac{x_i - x_0}{d_{i,j}}\hat{x} + \frac{y_i - y_0}{d_{i,j}}\hat{y}\right) \tag{2.1}$$

The total repulsive force exerted on the robot is determined by summing the active cells, shown in Equation 2.2

$$\overrightarrow{F_r} = \sum_{i,j} \overrightarrow{F_{i,j}} \tag{2.2}$$

$$\overrightarrow{F_t} = F_{ct}\left(\frac{x_t - x_0}{d_t}\hat{x} + \frac{y_t - y_0}{d_t}\hat{y}\right) \tag{2.3}$$

Summing together attractive and repulsive forces produce a vector $\overrightarrow{R}$ that can be used for heading guidance, shown in Equation 2.4.

$$\overrightarrow{R} = \overrightarrow{F_r} + \overrightarrow{F_t} \tag{2.4}$$

Major drawbacks to potential field were identified in [15] consisting of local minimum and oscillations in corridors. The local minimum problem occurs when closely spaced obstacle's potential combine to produce a well on the descent gradient where a pre-mature stable point is reached, shown in Figure 2.7. Additionally, closely spaced obstacles may also be difficult to pass between, shown in Figure 2.8a. Oscillations can also be experienced near obstacles or in narrow passages at high speeds, shown in Figure 2.8b.

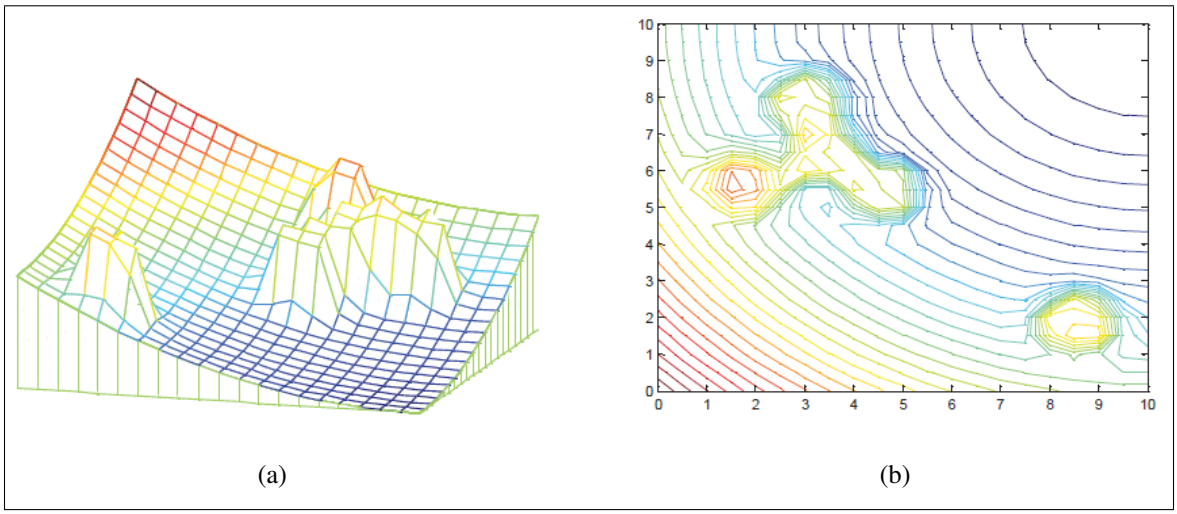

Figure 2.7: Potential Field Local Minimum [12]

Proposed solutions to local minimum include object clustering and virtual waypoint method [12], virtual escaping route [16], and use of navigation functions [17]. Oscillations in potential field were addressed in [18] and [19].

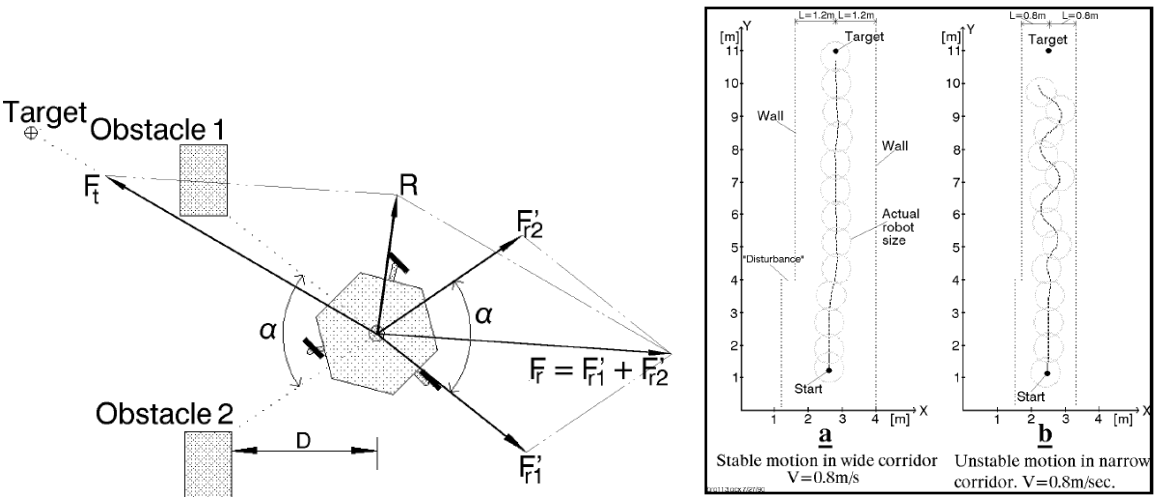

Figure 2.8: Potential Field Local Minimum [12]

Navigation functions [17] and obstacle clustering [12] have been used to prevent local minimums in potential field. Navigation functions relate kinematic constraints to the gradient potential to produce a bounded and local minimum free solution [11]. Clustering closely spaced obstacles into a single and equally repulsive obstacle prevents local minimum from forming, shown in Figure 2.9.

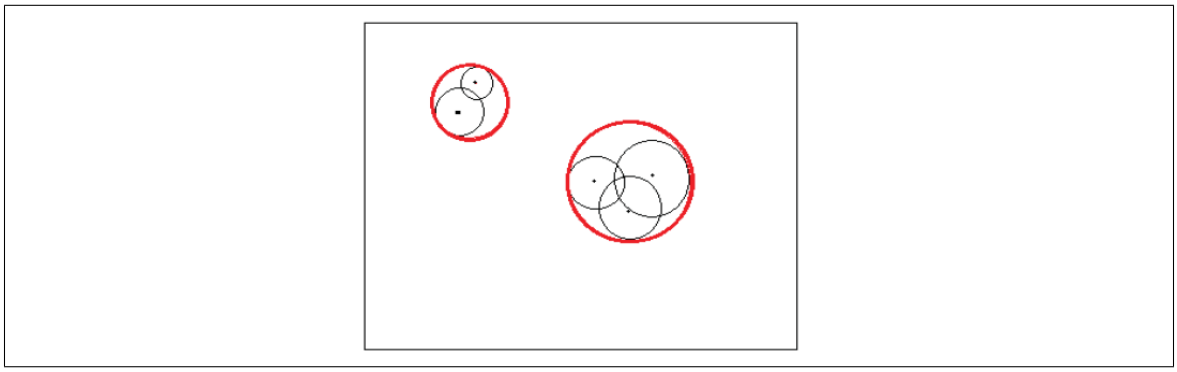

Figure 2.9: Obstacle Clustering [12]

Potential Field's ability to avoid obstacles and combine path planning, trajectory planning, and control into a single computationally inexpensive system makes it an attractive motion control system for robots seeking a singular point, even with the limitations discussed in [15].

In addition to local minimum and oscillations, potential field may not be ideal for providing guidance to return to a sensor path after avoiding an obstacle. Unlike the mobile ground robots in [13], fixed wing UAVs must maintain a minimum forward velocity, have limited turning radius, and cannot converge to a single point. Vehicles with velocity and turn rate constraints may not return to a pre-planned path once the obstacle has been avoided, shown in Figure 2.10. Vector fields that direct a UAV to paths connecting waypoints have been developed using Lyapunov and gradient vector field techniques.

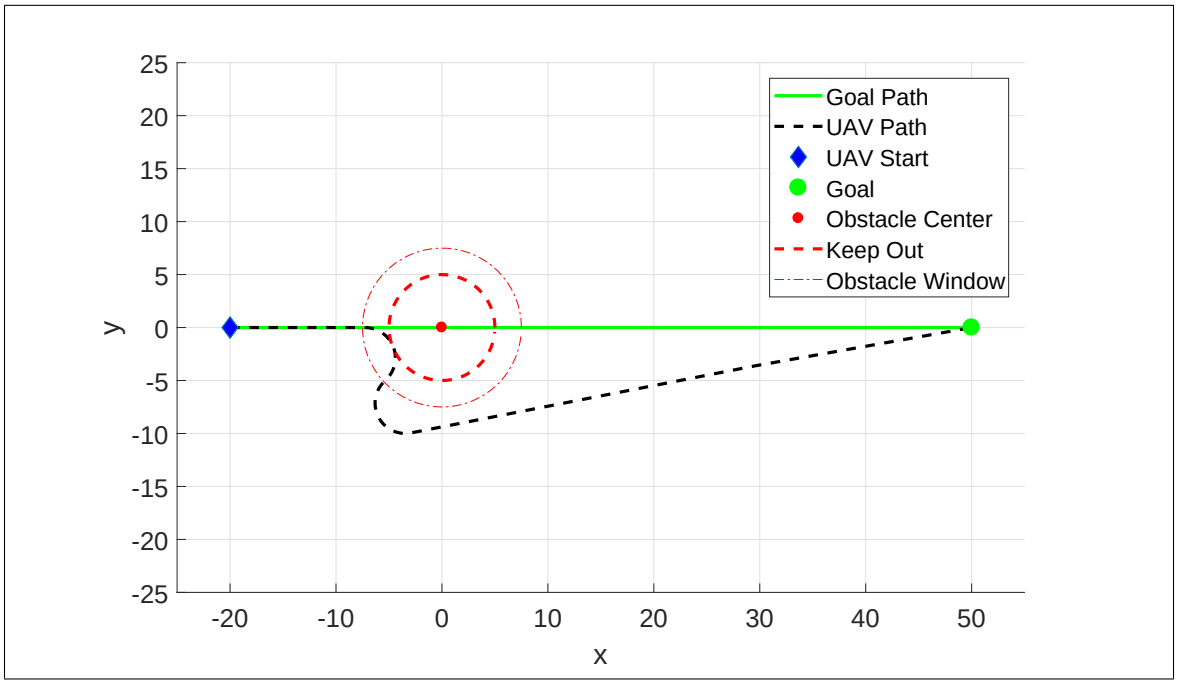

Figure 2.10: UAV avoiding obstacle with VFF Guidance

2.4.2 Lyapunov Vector Fields

Lyapunov vector fields for converging and following straight and circular paths were described in [20]. For converging and following a straight path, a guidance vector χ^d is determined in Equation 2.5, where χ^∞ is the course approach angle, y is the lateral distance to the path, and k is a positive constant that determines the rate of transition between convergence and following. An example of a Lyapunov vector field converging and following a straight line is shown in Figure 2.11a.

$$\chi^d(y) = -\chi^\infty \frac{2}{\pi} \tan^{-1}(ky) \tag{2.5}$$

For converging and following a circular path, a guidance vector χ^d is determined in Equation 2.6, where γ is the UAVs angular position with respect to the circle, r is the paths radius, d is the distance from the circles center, and k is a positive constant that determines the transition behavior. An example of a Lyapunov vector field for converging and following a circular path is shown in Figure 2.11b.

$$\chi^d(d) = \gamma - \frac{\pi}{2} - \tan^{-1}\left(k\frac{d-r}{r}\right) \tag{2.6}$$

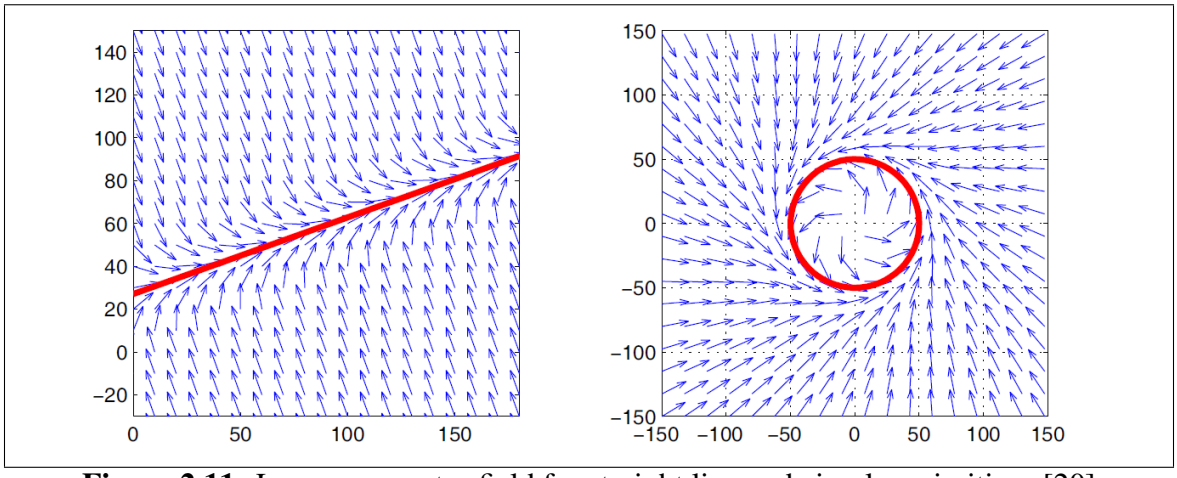

Figure 2.11: Lyapunov vector field for straight line and circular primitives [20]

Straight and circular path vector fields can be selectively activated throughout flight to form more complex paths, shown in [20–23] and Figure 2.12. Each path primitive has a vector field associated with it and determining which field to use can be approached in two different ways. Fields from all of the primitives can be summed together similar to the attractive and repulsive forces in potential field. Second, fields can be selectively activated and deactivated based on the position of the UAV. Summing together vector fields, as pointed out in [20], can result in several problems including dead zones, sinks, and singularities. Selectively activating each vector field as a UAV nears waypoints was used in [20–23].

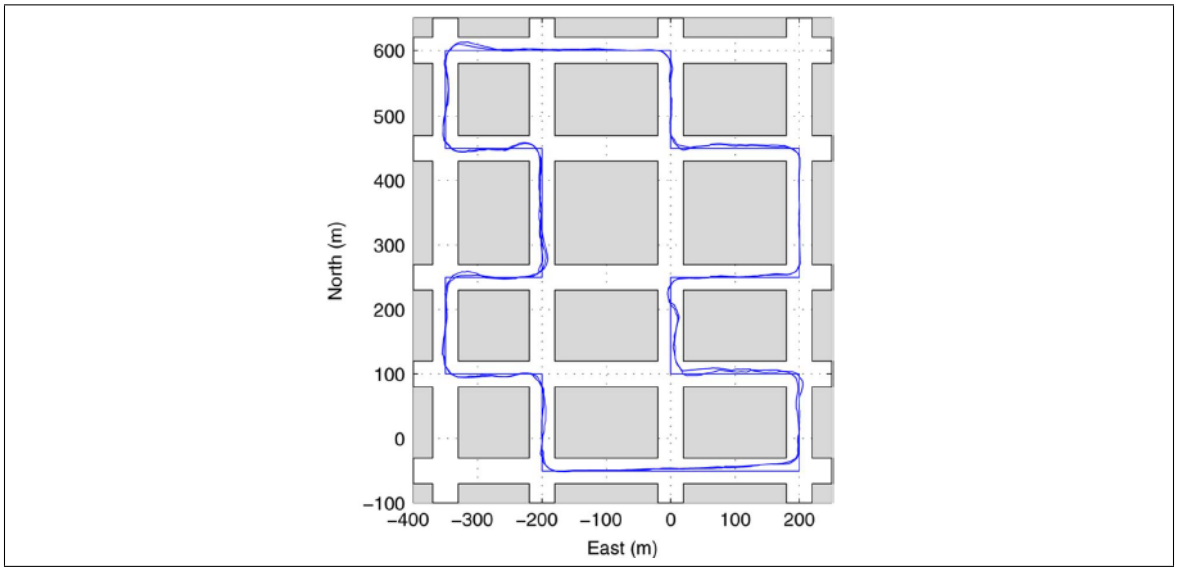

Figure 2.12: Straight path following in urban environment [20] using Lyapunov Vector Field

Lyapunov Vector field construction for curved paths was presented in [24] and is shown in Figure 2.13. Constructing a Vector Field for an arbitrary curve may allow for more complex paths and could eliminate the need for switching between primitives.

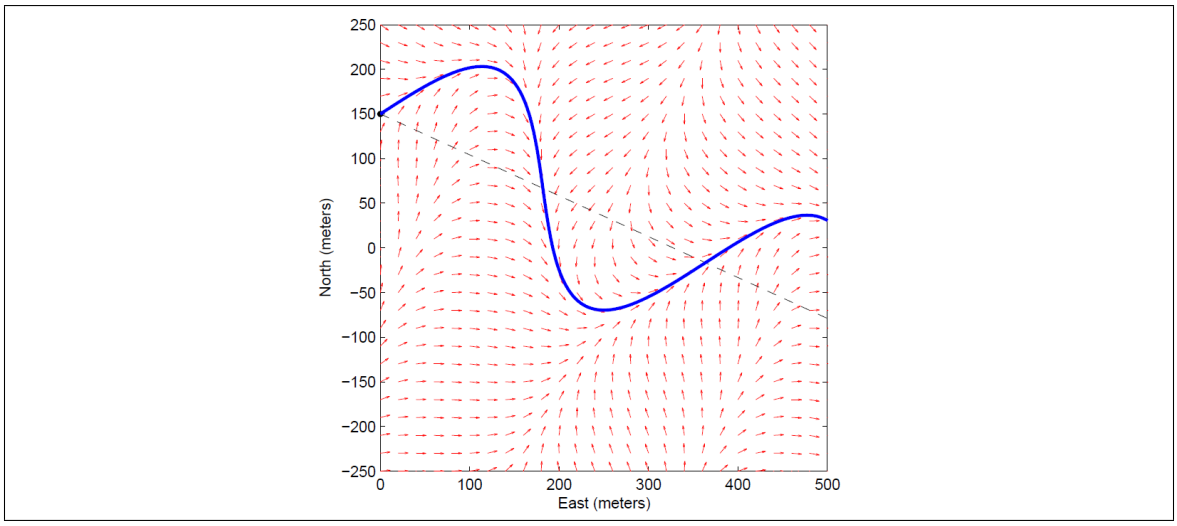

Figure 2.13: Lyapunov vector field approach curved path asymptotically [24]

Primitive circular vector fields were modified in [25, 26] via non-linear coordinate transformations to produce elliptical 2.14a, or racetrack 2.14b, fields. Transforming the circular field as a function of a Kalman filter's covariance matrix when sensing an uncertain target was investigated in [26].

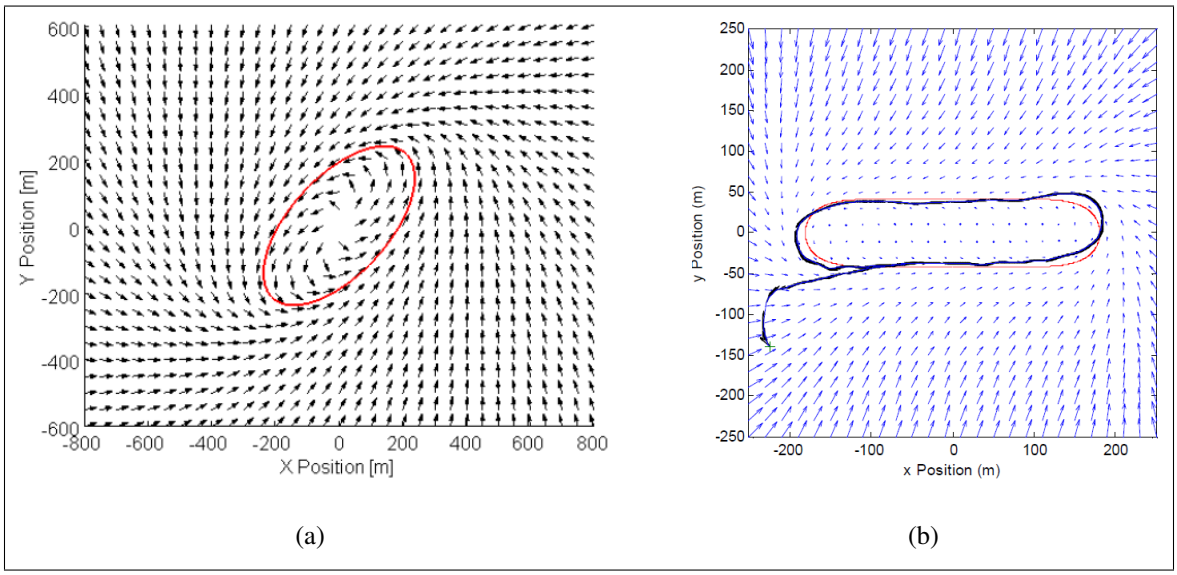

Figure 2.14: Elliptical VF produced by non-linear coordinate transformations a) [26] and b) [25]

Target tracking Tangent Plus Lyapunov Vector Field (TPLVF) was introduced in [27] that produced shorter paths compared to Lyapunov alone. Outside of the standoff circle, tangent vectors provided the shortest distance to a standoff circle. Inside the standoff circle, no tangent lines exist and Lyapunov was used in its place. Figure 2.15 shows the difference in paths taken for Lyapunov and tangent vector fields outside the standoff circle. The TPLVF was later used for path planning to avoid obstacles in [28] while [29] constructed a tangent vector field for curved paths.

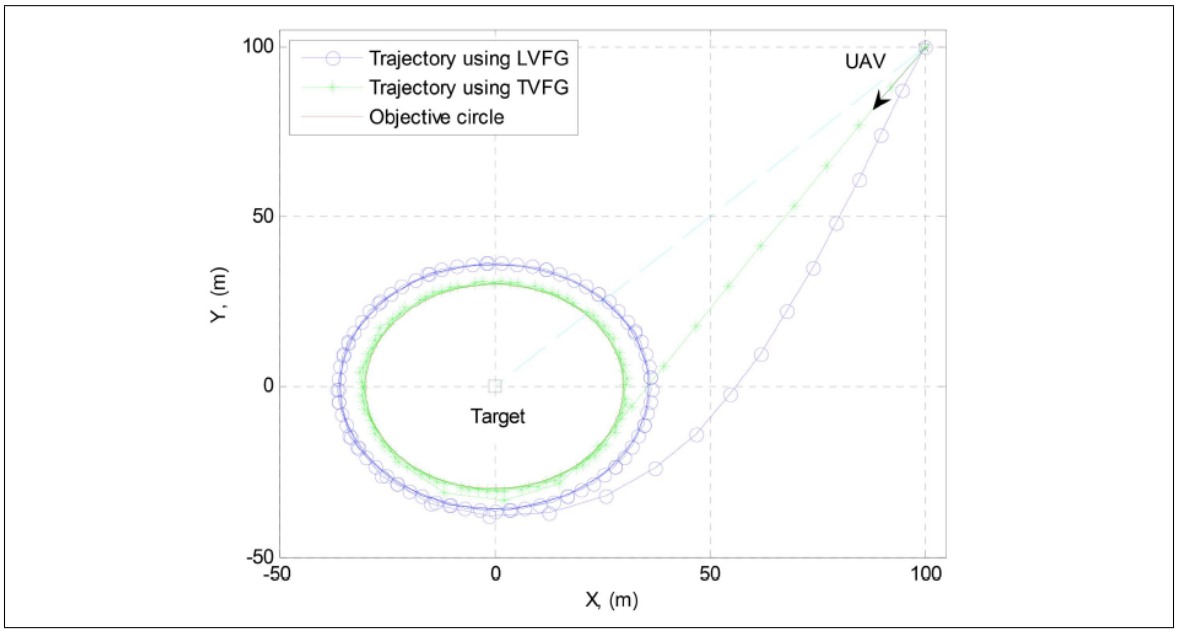

Figure 2.15: Tangent plus lyapunov vector fields for shortest path target tracking [28]

2.4.3 Path Planning Vector Fields

All methods that consider obstacles thus far built a vector field that guides the UAV to an obstacle free path. Another approach is to use vector fields as a high level specification for heuristic path planning algorithms [30]. An optimal Rapid Random Trees (RRT*) algorithm used a vector field as a guide to explore the configuration space of the UAV for an obstacle free path. Branches extend from the root, or initial location of the UAV,

randomly throughout the map with a finite deviation from the initial vector field. When a branch encounters an obstacle it is trimmed and no longer explored. The path of minimum cost, or least distance, is selected for the UAV to use as a reference path. An example of the algorithm is shown in Figure 2.16.

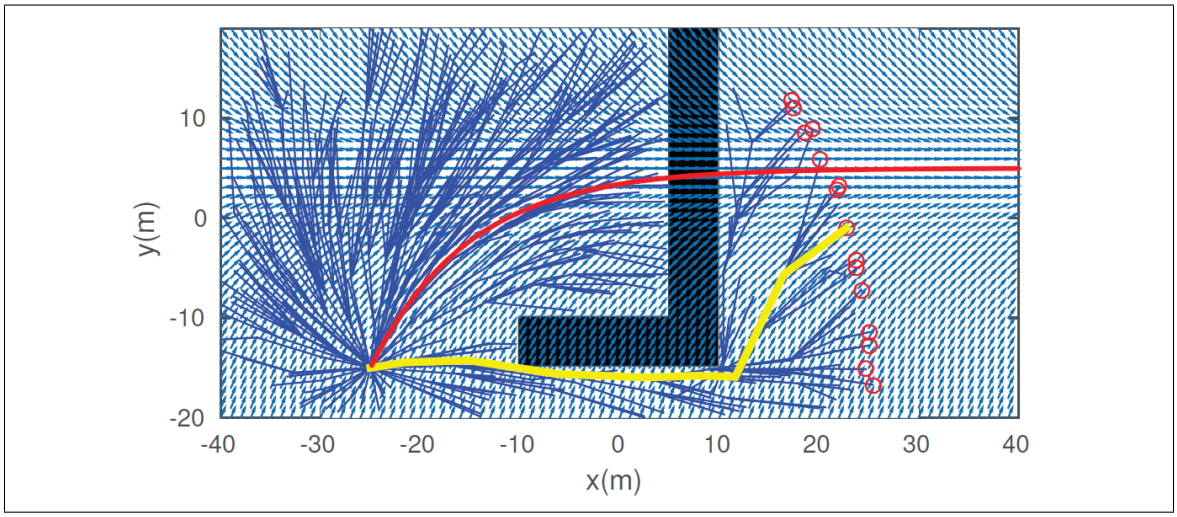

Figure 2.16: RRT* path planner with a VF used as a task specification [30]

A Vector Field was constructed inside a configuration space with edges defined by Delauny triangulation (DT) in [31]. A simulation of a robot traversing a vector field inside a set of DTs can be seen in Figure 2.17. Vector fields designed to stay inside a region of DTs may be used with optimal path planning algorithms for navigating urban environments [32].

So far all of the vector field methods discussed have avoided obstacles by planning paths around them. Paths are typically calculated at the ground station and if communication is lost a new path may not be relayed to a UAV encountering a new obstacle. A possible solution is using vector fields to provide a repulsive force such as that seen in [2, 33] [wwc].

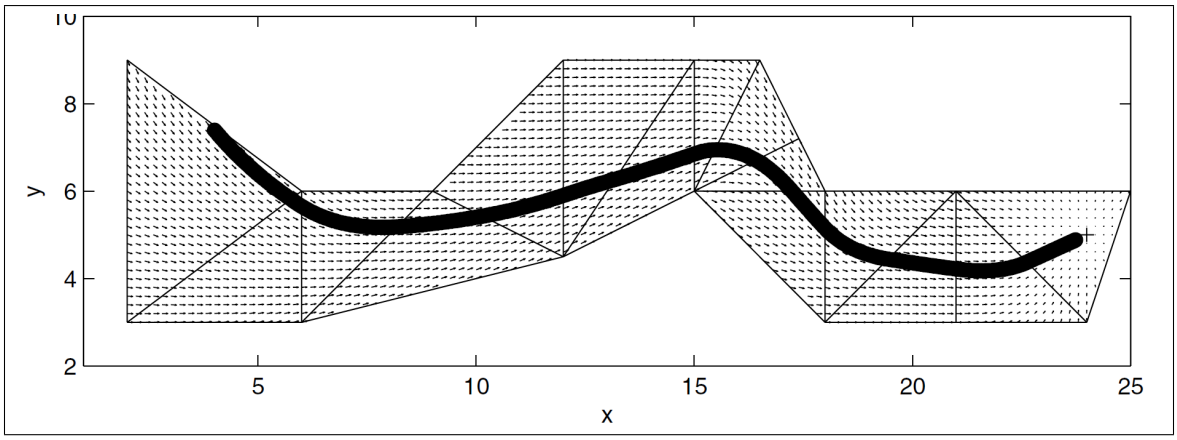

Figure 2.17: Vector field within a set of delaunay triangles [31]

2.4.4 Gradient Vector Field

The Gradient Vector Field (GVF) method produces a similar field to LVF, however has several advantages over LVFs. GVF produces an n-dimensional vector field that converges and circulates to both static and time varying paths [34]. Additionally, convergence, circulation, and time-varying terms that make up the GVF are decoupled from each other allowing for easy weighting of the total field [35]. GVFs converge and circulate at the intersection, or level set, of $n-1$ dimensional implicit surfaces ($\alpha_i : \mathbb{R}^n \rightarrow \mathbb{R} | i = 1, ..., n-1$). The integral lines of the field are guaranteed to converge and circulate the level set when two conditions are met: 1) the implicit surface functions are positive definite and 2) have bounded derivatives. Consider the space with dimensions in set $\mathbf{q}$:

$$\mathbf{q} = \left[x_1, x_2, ..., x_n \right] \tag{2.7}$$

The total vector field $\overrightarrow{V}$ is calculated by:

$$\overrightarrow{V} = G\nabla V + H \wedge_{i=1}^{n-1} \nabla_q \alpha_i - LM(\alpha)^{-1} a(\alpha) \tag{2.8}$$

or in component form:

$$\overrightarrow{V} = \overrightarrow{V}_{conv} + \overrightarrow{V}_{circ} + \overrightarrow{V}_{tv} \tag{2.9}$$

where $\overrightarrow{V}_{conv}$ produces vectors perpendicular to the path, $\overrightarrow{V}_{circ}$ produces vectors parallel to the path, and $\overrightarrow{V}_{tv}$ is a feed-forward term that produces vectors accounting for a time varying path. The scalars G,H, and L weight convergence, circulation, and time varying components respectively.

Convergence is calculated by:

$$\overrightarrow{V}_{conv} = G\nabla V \tag{2.10}$$

where scalar G is multiplied by the gradient of the definite potential function V:

$$V = -\sqrt{{\alpha_1}^2 + {\alpha_2}^2} \tag{2.11}$$

Circulation is calculated by taking the wedge product of the gradient:

$$\overrightarrow{V}_{circ} = \wedge_{i=1}^{n-1} \nabla_q \alpha_i \tag{2.12}$$

In the case of ($n = 3$) the wedge product simplifies as the cross product:

$$\overrightarrow{V}_{circ} = \nabla_q \alpha_1 \times \nabla_q \alpha_2 \tag{2.13}$$

The feed-forward time-varying component is calculated by:

$$\overrightarrow{V}_{tv} = M^{-1} a \tag{2.14}$$

where,

$$M = \begin{bmatrix} \nabla \alpha_1^T \\ \nabla \alpha_2^T \\ (\nabla \alpha_1 \times \nabla \alpha_2)^T \end{bmatrix} \tag{2.15}$$

$$a = \begin{bmatrix} \frac{\partial \alpha_1}{\partial t} & \frac{\partial \alpha_2}{\partial t} & 0 \end{bmatrix}^T \tag{2.16}$$

In [34–36] GVFs h were constructed to control the velocity $\dot{q}$ of holonomic robots by $\dot{q} = h$. Constant speed u was controlled by calculating the weighting scalars G,H, and L that maintained the condition $||\dot{q}|| = u$. Other studies normalized the vector $\overrightarrow{V}$ and used it as a heading guidance while assuming velocity is held constant by the autopilot [**?**, 37]. Assuming velocity is controlled by a separate system frees up the vector field scalars to modify field behavior for other applications, such as obstacle avoidance.

The standoff tracking and avoidance scenario presented in [**?**] used GVF as a heading guidance and static GVF weights to specify high level guidance behavior. A fixed UAV was tasked with loitering around a slow moving ground target while avoiding obstacles. A circular attractive time-varying vector field $\overrightarrow{V}_{path}$ was attached to a moving ground target and summed with repulsive obstacle vector fields $\overrightarrow{V}_o$ centered at the obstacles to provide the guidance $\overrightarrow{V}$ in Equation 2.17.

$$\overrightarrow{V} = \overrightarrow{V}_{attractive} + P\overrightarrow{V}_{repulsive} \tag{2.17}$$

The strength of repulsive obstacle fields were weighted by the hyperbolic tangent decay function $P(d)$ in Equation 2.18, where d is the range to the obstacle and R is the radius of the decay

$$P = R\frac{tanh(2\pi d - \pi) + 1}{2} \tag{2.18}$$

The performance of LVF [21] and GVF [34–36] were compared for their cross track error with respect to the loiter circle in [wwc]. GVF had favorable performance due to compensation for a time-varying vector field. The path of the fixed wing UAV tracking a slow moving ground target while avoiding static obstacles is shown in Figure 2.18

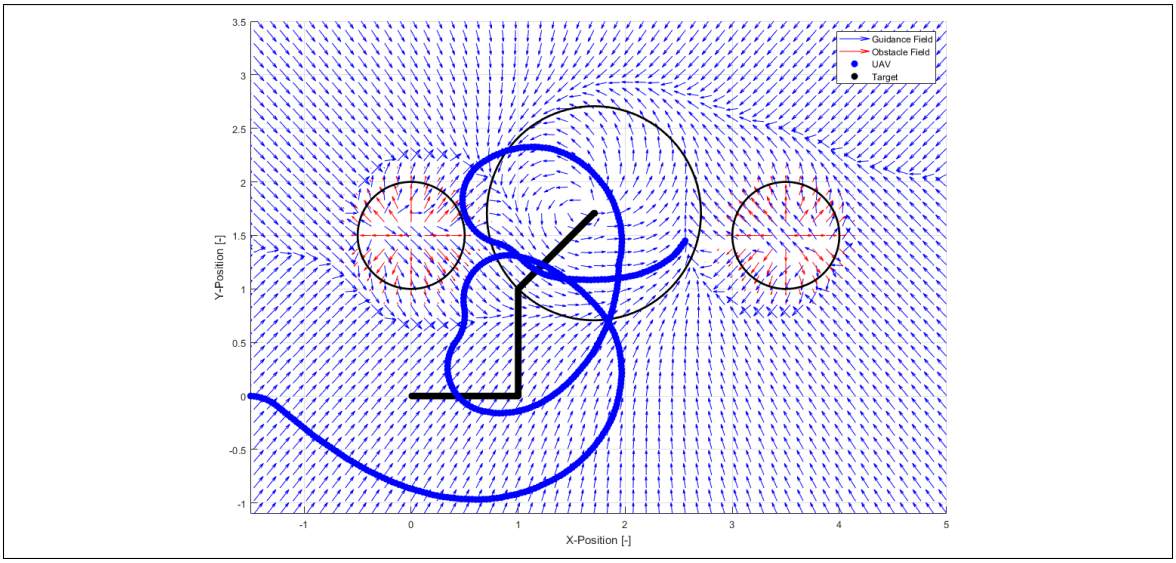

Figure 2.18: Place holder image of UAV following ground target [**?**]

Summing attractive and repulsive vector fields may result in null guidance where the fields cancel, providing no guidance. The presence of singularities were not addressed in [**?**], mentioned briefly in [20] and observed in [2]. For fixed wing UAVs the lack of guidance may prevent the UAV from avoiding an obstacle, while multi-rotor UAVs may end up in a trap situation. Singularities may be present at any location where a goal field and obstacle field are of equal strength. Detecting singularities and modifying the GVF for an improved obstacle avoidance is the contribution of this research.

2.5 Literature Review Summary

Vector fields can provide guidance and control for robots through the use of artificial attractive and repulsive forces. Converging to a singular point while avoiding obstacles can be achieved with Potential Field or Virtual Force Field methods. Fixed wing UAVs cannot converge to a singular point therefore vector fields that asymptotically converge and follow a path is beneficial. Lyapunov and Gradient Vector Fields have been used for path following, standoff tracking, and obstacle avoidance. Gradient Vector Field provides

convenient and decoupled access to scalar multiplicative weights for the convergence, circulation, and time-varying terms. Negative weights can be used for obstacle avoidance, however have so far been used only as high level specification of guidance behavior. Specifying vector field weights as functions of a UAV's state may enable an optimal guidance for obstacle avoidance. Validation of a modified GVF guidance can be performed on mobile ground robots simulating UAV dynamics.

3 METHODOLOGY

3.1 Introduction to Methodology

A real-time circular obstacle avoidance guidance is achieved by summing together a path following and obstacle avoidance vector field with optimized decay and circulation weights. Singularities in summed vector fields are defined and a method for numerically locating their position is presented in Phase I and it is shown how adding circulation to repulsive GVFs may remove singularities from the UAVs path. Phase II investigates a method for selecting the combination of repulsive GVF decay radius and circulation weights that minimizes a path deviation cost function. The optimized GVF guidance is implemented on an indoor multirotor UAV operating under fixed wing constraints in Phase III.

3.2 Phase I: Gradient vector field singularity detection

The objective of Phase I is to characterize and present a method for locating singularities in a summed gradient vector field in simulation. Phase I consists of calculating guidance for converging and following a straight path using the GVF method in literature. An obstacle field is constructed for avoiding circular obstacles along the path by modifying GVF's convergence and circulation weights. Summing the attractive and repulsive GVFs results in guidance that guides the UAV along the planned path while pushing away from an obstacle. Regions in the summed guidance where the path following and obstacle guidance directly oppose each other, called singularities, result in vectors of zero length. A method for identifying the location of singularities is presented along with a method for mitigating them.

3.2.1 Path Following Vector Field Guidance

Guidance for converging and following a path using GVF guidance is achieved by summing together convergence and circulation terms that are multiplied by scalars G and H respectively, shown in Equation 3.1. The potential function V, Equation 3.2 decreases asymptotically to null when approaching the target path and therefore the convergence vector begins to decrease as well. As the potential function decreases, the circulation term begins to dominate the guidance, promoting path following. How close to the target path the transition between convergence and circulation depends on the scalar weights G and H respectively.

$$\overrightarrow{V} = G\nabla V + H(\nabla\alpha_1 \times \nabla\alpha_2) \tag{3.1}$$

$$V = -\sqrt{{\alpha_1}^2 + {\alpha_2}^2} \tag{3.2}$$

Equation 3.1 for straight path following will be represented in component form for convenience, shown in Equation 3.8. The total vector $\overrightarrow{V}_p$ represents the non-normalized attractive path following vector comprised of both convergence and circulation terms.

$$\overrightarrow{V}_p = G\overrightarrow{V}_{conv} + H\overrightarrow{V}_{circ} \tag{3.3}$$

The shape of the target path that the vectors converge and follow depend on the specification of the implicit 3-dimensional surface functions α_1 and α_2. Intersecting two planes, shown in Figure 3.1, can be used to generate a GVF that converges and follows a straight path. The vertical plane, described in Equation 3.4, at angle δ is intersecting with a horizontal plane at constant height z, Equation 3.5

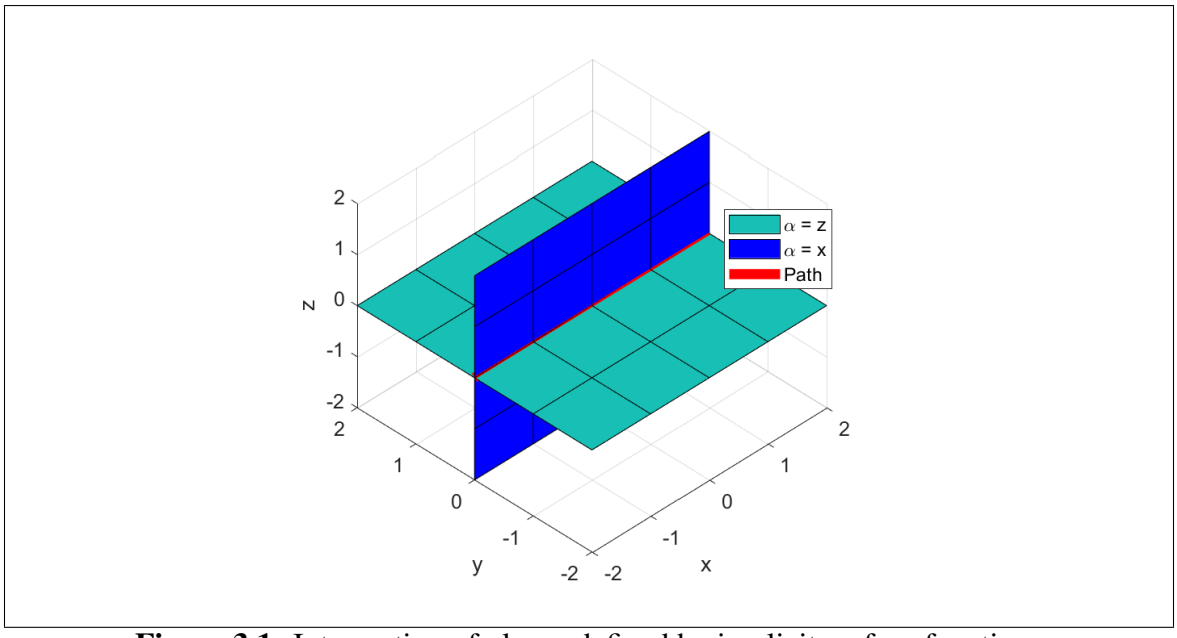

Figure 3.1: Intersection of planes defined by implicit surface functions

$$\alpha_1 = cos(\delta)x + sin(\delta)y \tag{3.4}$$

$$\alpha_2 = z \tag{3.5}$$

The gradient potential, ∇V, for calculating the path following convergence term is shown in Equation 3.6.

$$\nabla V = -\frac{1}{2(\sqrt{\cos^2(\delta)x^2 + 2\cos(\delta)\sin(\delta)xy + \sin^2(\delta)y^2})} \begin{bmatrix} 2x\cos^2(\delta) + 2\cos(\delta)\sin(\delta)y \\ 2y\sin^2(\delta) + 2\cos(\delta)\sin(\delta)x \\ 2 \end{bmatrix} \tag{3.6}$$

Circulation is calculated by the cross product of the surface function gradients, which evaluates to that shown in Equation 3.7.

$$\overrightarrow{V}_{circ} = \begin{bmatrix} sin(\delta) \\ -cos(\delta) \\ 0 \end{bmatrix} \tag{3.7}$$

Prior to using the path following guidance $\overrightarrow{V}_p$, it is normalized to have a magnitude $||\overrightarrow{V}_p|| = 1$. The reason for normalizing the vector is threefold. First, the vector is used as a heading controller only, therefore the angle of the vector is the necessary information. Second, the normalized vectors result in quiver plots with equal density arrows making the field easier to visualize. Lastly, normalizing the path following vector $\overrightarrow{V}_p$ fixes the length of the vector allowing for prediction of singularity location after summing the field, which will be discussed in the next section. Before discussing singularities, the obstacle field is introduced.

$$\overrightarrow{V}_{||P||} = \frac{\overrightarrow{V}_p}{||\overrightarrow{V}_p||} \tag{3.8}$$

To produce guidance for following a path and avoiding an obstacle, a repulsive obstacle vector field $\overrightarrow{V}_{||O||}$ needs to be constructed and summed with the normalized path following guidance $\overrightarrow{V}_{||P||}$. The repulsive vector field is multiplied by a decay function P which limits the influence of the obstacle to a finite range and will be discussed after the avoidance field equations are presented. The sum of the two guidances is represented by $\overrightarrow{V}_g$ and is shown in Equation 3.9

$$\overrightarrow{V}_g = \overrightarrow{V}_{||P||} + P\overrightarrow{V}_{||O||} \tag{3.9}$$

Constructing the obstacle avoidance vector field will now be discussed.

3.2.2 Constructing an Avoidance Vector Field

A circular avoidance vector field will now be constructed in a way similar to that of the path following field in the previous section. What differentiates the obstacle field from the path following field is that the individual convergence and circulation components are normalized prior to normalizing the summed obstacle field $\overrightarrow{V}_o$. The benefit of normalized each field component before multiplying by their respective scalars and summing is to produce a obstacle field with uniform behavior as distance from the obstacle increases. In short, normalizing each component allows both convergence and circulation terms to be present in the obstacle guidance at larger distances. Additionally, negative convergence weights will be used to produce vectors that diverge away from the path. The obstacle vector field is constructed using the normalized component Equation 3.10 with obstacle convergence and circulation weights G_o and H_o respectively.

$$\overrightarrow{V}_o = G_o \frac{\overrightarrow{V}_{conv}}{\|\overrightarrow{V}_{conv}\|} + H_o \frac{\overrightarrow{V}_{circ}}{\|\overrightarrow{V}_{circ}\|} \tag{3.10}$$

A circular avoidance vector field with radius r centered at (x_c, y_c) is constructed by intersecting a cylinder, Equation 3.11, and a plane Equation 3.5.

$$\alpha_1 = (x - x_c)^2 + (y - y_c)^2 - r^2 \tag{3.11}$$

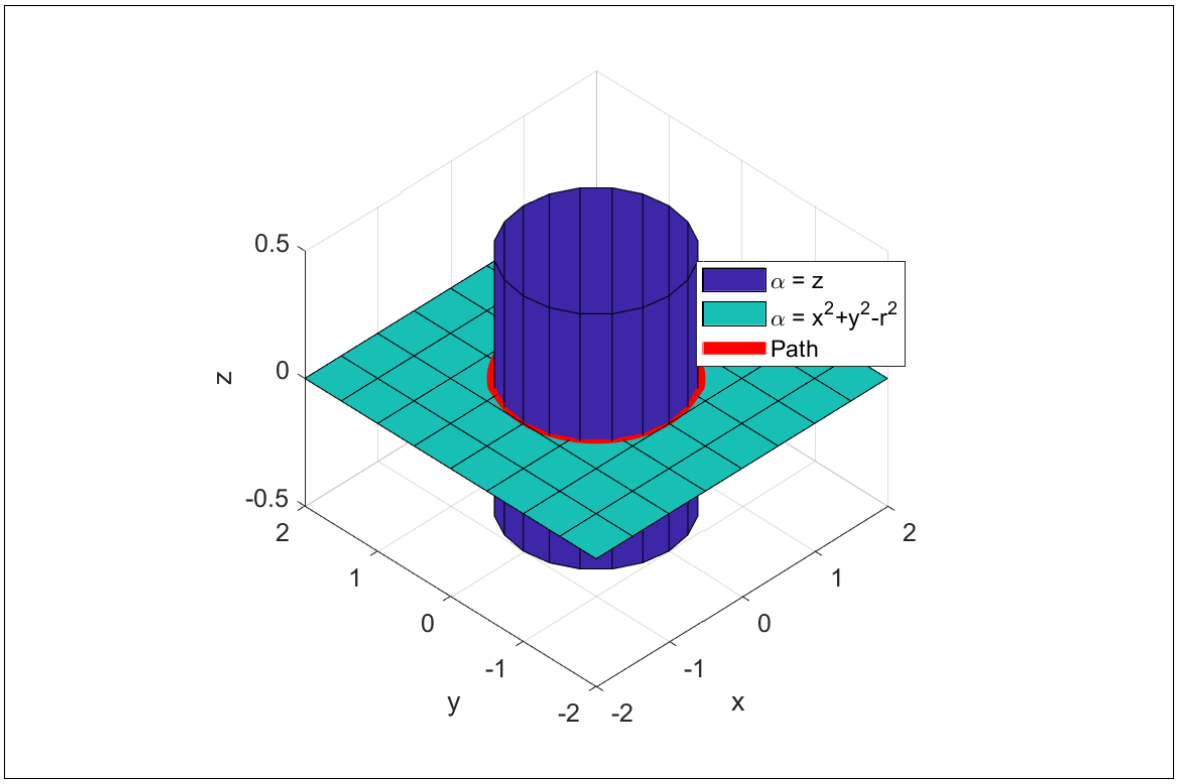

Figure 3.2: Intersection of a cylinder and plane defined by implicit surface functions

Convergence is calculated by the gradient of the potential function 3.6, which when simplified evaluates to

$$\nabla V = A\vec{B} \tag{3.12}$$

where

$$A = \frac{-1}{\sqrt{\bar{x}^4 + \bar{y}^4 + 2\bar{x}^2\bar{y}^2 - 2r^2\bar{x}^2 - 2r^2\bar{y}^2 + r^2 + z^2}} \tag{3.13}$$

$$\vec{B} = \begin{bmatrix} 2\bar{x}^3 + 2\bar{x}\bar{y}^2 - 2r^2\bar{x} \\ 2\bar{y}^3 + 2\bar{x}^2\bar{y} - 2r^2\bar{y} \\ z \end{bmatrix} \tag{3.14}$$

and

$$\bar{x} = x - x_c \tag{3.15}$$

$$\bar{y} = y - y_c \tag{3.16}$$

Evaluating equation 3.12 results in a vector field that converges to a circular path. Circulation is calculated from the cross product of each implicit surface function's gradient, which simplifies to

$$\overrightarrow{V}_{circ} = \begin{bmatrix} 2(y - y_c) \\ -2(x - x_c) \\ 0 \end{bmatrix} \tag{3.17}$$

Obstacle fields should only act locally on a UAV guidance which is accomplished by applying a decay function for a field of radius R. The decay strength P is determined in 3.18, where d is the euclidean distance, or range, between the UAV and the center of the obstacle, shown in Equation 3.19. At a distance $d > R$ the decay strength P is effectively zero, having virtual no influence on the total guidance. At a distance $d \leq R$, the field strength is bounded between $[0, 2]$. The selection of the decay function P to be bounded as such is so that the obstacle field $\overrightarrow{V}_o$ eventually overpowers the path field $\overrightarrow{V}_{\|P\|}$. A plot of the decay function in Equation 3.18 is shown in Figure 3.19.

$$P = -\tanh\left(\frac{2\pi d}{R} - \pi\right) + 1 \tag{3.18}$$

$$d = \sqrt{\bar{x}^2 + \bar{y}^2} \tag{3.19}$$

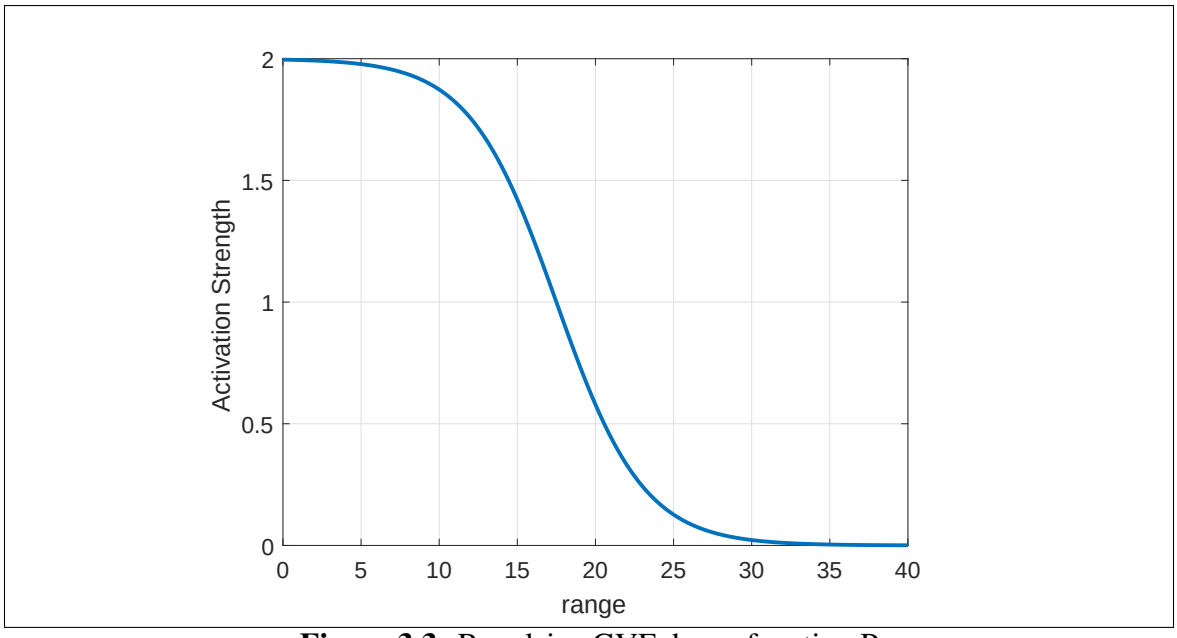

Figure 3.3: Repulsive GVF decay function P

Prior to applying the decay function the sum of obstacle field's convergence and circulation terms are normalized to ensure the vector's magnitudes are of length unity, shown in Equation 3.20.

$$\overrightarrow{V}_{\|o\|} = \frac{\overrightarrow{V}_o}{\|\overrightarrow{V}_o\|} \tag{3.20}$$

3.2.3 Summed Guidance and Singularity Definition

The total summed guidance $\overrightarrow{V}_g$ defined in Equation 3.9 can now be calculated and visualized, Figure 4.9. In general, the GVF guidance is more easily visualized if the final guidance is normalized yet again, however, plotting the path following and obstacle guidance $\overrightarrow{V}_g$ demonstrates regions where the fields oppose each other, possibly leading to GVF singularities. For a strictly repulsive field that is centered on a straight path, regions of both constructive and destructive summation occurs. Note the vectors on the positive x-

axis increasing in length as the two fields come together. Conversely, vectors in the negative x-axis show decreasing length and in some areas disappearing entirely.

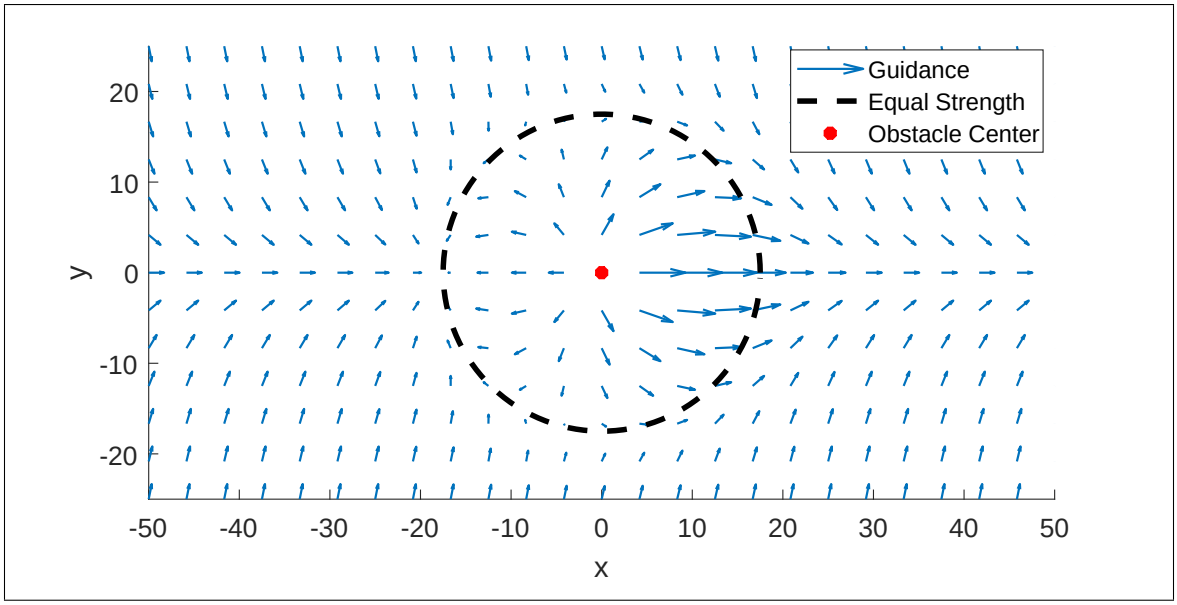

Figure 3.4: Summed fields without total normalization $\overrightarrow{V}_g$

It appears that the regions leading up to the singularities have vectors that guide towards the singularities. Opposing vectors that lead into a well may produce trap situations where a UAV may be unable to escape if continuing to use GVF guidance. The location of the singularities can be approximated by plotting the magnitude of the summed field near the obstacle.

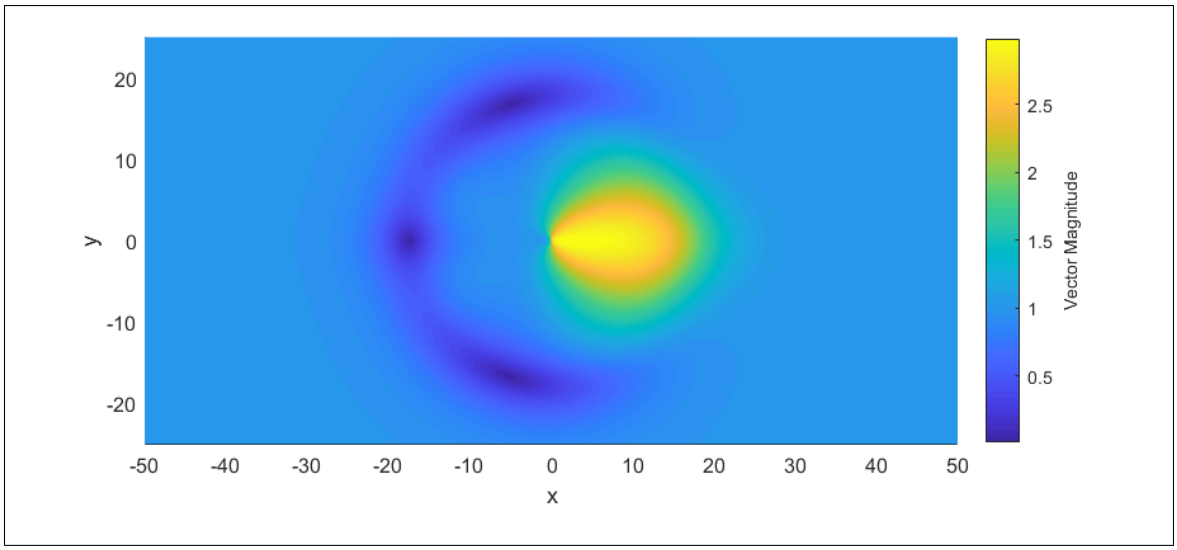

Figure 3.5: Summed Fields Without Total Normalization

Singularities may be used to detect these regions and possibly protect UAVs from entering trap situations. Singularities in the vector field are defined as a region in the GVF space where the vector has zero magnitude, shown in Equation 3.21.

$$||\overrightarrow{V}_g|| = 0 \tag{3.21}$$

By extension, singularities are a result of a zero vector, shown in Equation 3.22 and Equation 3.23.

$$\overrightarrow{0} = \overrightarrow{V}_{||P||} + P\overrightarrow{V}_{||O||} \tag{3.22}$$

$$\overrightarrow{V}_{||P||} = -P\overrightarrow{V}_{||O||} \tag{3.23}$$

Vectors $\overrightarrow{V}_{||P||}$ and $\overrightarrow{V}_{||O||}$ are normalized, meaning that their magnitudes are of equal length $||\overrightarrow{V}_{||P||}|| = ||\overrightarrow{V}_{||O||}||$. For the condition shown in Equation 3.23 to be true for an obstacle field with a negative convergence weight $G = -1$, the decay function P must be unity.

Setting Equation 3.18 equal to 1, the distance at which the fields have equal strength is determined to be that shown in Equation 3.24

$$d = \frac{R}{2} \tag{3.24}$$

An example of using a numerical solver with various initial conditions placed along a radius of $d = r/2$ is shown in Figure 3.6

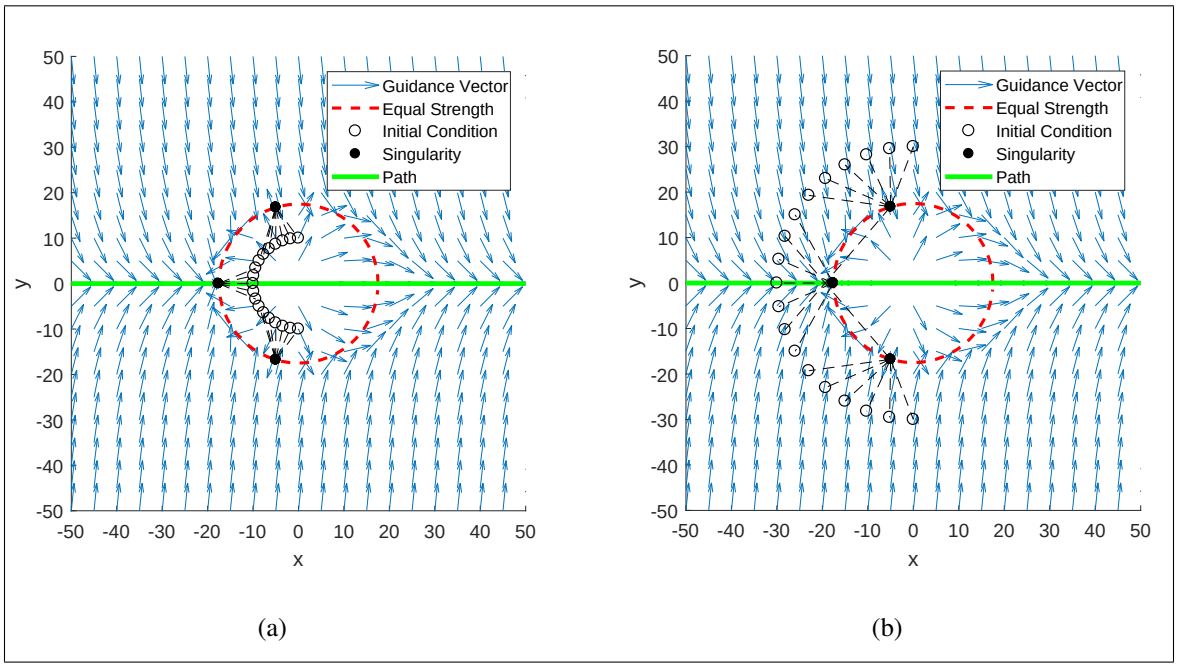

Figure 3.6: GVF converging and circulating circular path

The method for constructing path following and obstacle GVFs will be used in Phase II along with singularity detection.

3.3 Phase II

The objective of Phase II is to determine the combination of gradient vector field circulation and decay radius for least cost circular obstacle avoidance.

The dynamics of UAVs are often simplified when simulating guidance systems by modeling the UAV as a Dubin's vehicle [20–22, 24, 26]. It is assumed that the autopilots control system is capable of maintaining stability, speed u, and can turn the vehicle at a fixed turn rate $\dot{\theta}$. The position of the UAV $\overrightarrow{X}$ at time t is calculated from the integral of the velocity vector $\overrightarrow{U}$, Equation 3.26. Heading is an input from a guidance system, such as waypoint, potential field, or vector field.

$$\overrightarrow{U}(t) = u \begin{bmatrix} cos(\theta(t)) \\ sin(\theta(t)) \end{bmatrix} \tag{3.25}$$

$$\overrightarrow{X}(t) = \overrightarrow{U}dt + \overrightarrow{X}(t-1) \tag{3.26}$$

$$\dot{\theta} \leq 20deg/s \tag{3.27}$$

A UAV that travels at a constant speed and has a fixed turn rate $\dot{\theta}$ can be guided to converge and follow a straight path the GVF guidance introduced in Phase I. Demonstrated in Figure 3.7, a UAV at initial position $(-45, 20)$ and heading θ of 45° is shown converging and following a path by GVF guidance with weights $G = 1, H = 5$.

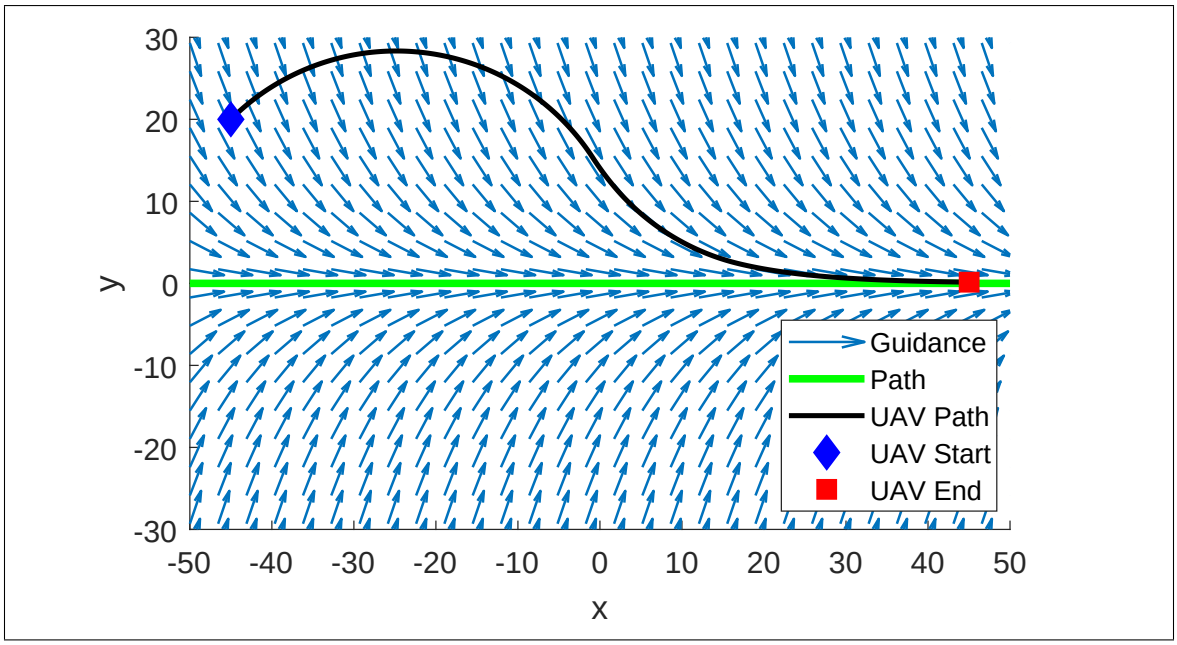

Figure 3.7: Fixed Wing converging and following a path

Obstacles along the pre-planned path are described using two parameters, the radius r_o and the lateral distance from the path y_o. It is assumed here that the radius of the obstacle is no smaller than the turn radius of the UAV θ_r, which is calculated in Equation 3.28. It is convenient to represent the obstacle's radius, Equation 3.29, as a multiple of the UAVs turning radius for reasons that will be discussed further into the methodology.

$$\theta_r = \frac{u}{\dot{\theta}} \tag{3.28}$$

$$r_o = n\theta_r \tag{3.29}$$

The repulsive vector field's decay radius R is defined in multiples of the obstacle's radius, shown in Equation 3.30. The decay function described in Equation 3.18 produces a circle of equal strength at $R/2$ centered on the obstacle. On this circle vectors from the repulsive field have the same magnitude as the path following vector fields. At the edge

and inside of the equal strength circle the repulsive guidance will begin to have significant impact on the total guidance.

$$R = kr_o \tag{3.30}$$

Strictly repulsive GVF obstacle fields can provide avoidance, however may cause excess deviation from the pre-planned path and unnecessary turns. The repulsive vectors directly and equally oppose the path following vectors shown in Figure 3.8.

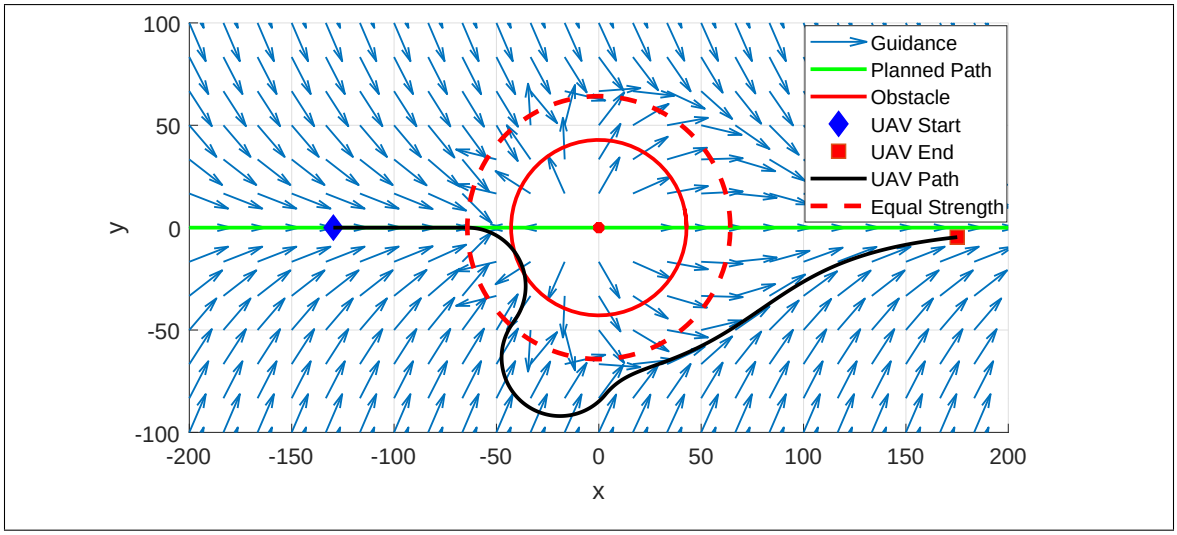

Figure 3.8: UAV encountering a circular obstacle centered on pre-planned path, no circulation

So far GVF weights and decay radii have been used as a high level specification of desired behavior, i.e pushing away from on obstacle region while circumnavigating a target [wwc]. Selecting obstacle GVF circulation H and decay radius R such that the deviation from a planned path is minimized would be beneficial in situations such as target tracking or surveying a sensor line. Additionally, it was shown in Phase I that adding circulation to a GVF can remove singularities from the GVF path.

A cost function can be used to measure the deviation from a planned path while avoiding an obstacle with GVF in Equation 3.31. The deviation, y, is the lateral distance of the UAV to the planned path, R is the obstacle radius, and the function j(x,y) increases the cost when the UAV violates the obstacles radius.

$$\gamma = \frac{1}{R}\int_0^{tf} ydt + j(x,y) \tag{3.31}$$

$$j(x,y) = \begin{cases} 100dt & \sqrt{(x-xc)^2+(y-yc)^2} \leq r_O \\ 0 & \sqrt{(x-xc)^2+(y-yc)^2} > r_O \end{cases} \tag{3.32}$$

The performance of a Dubin's UAV with a speed $u = 20m/s$ and turnrate $\dot{\theta}$ avoiding an obstacle of radius $2.5m$ with a range of circulation and decay radii R is shown in Figure 3.9.

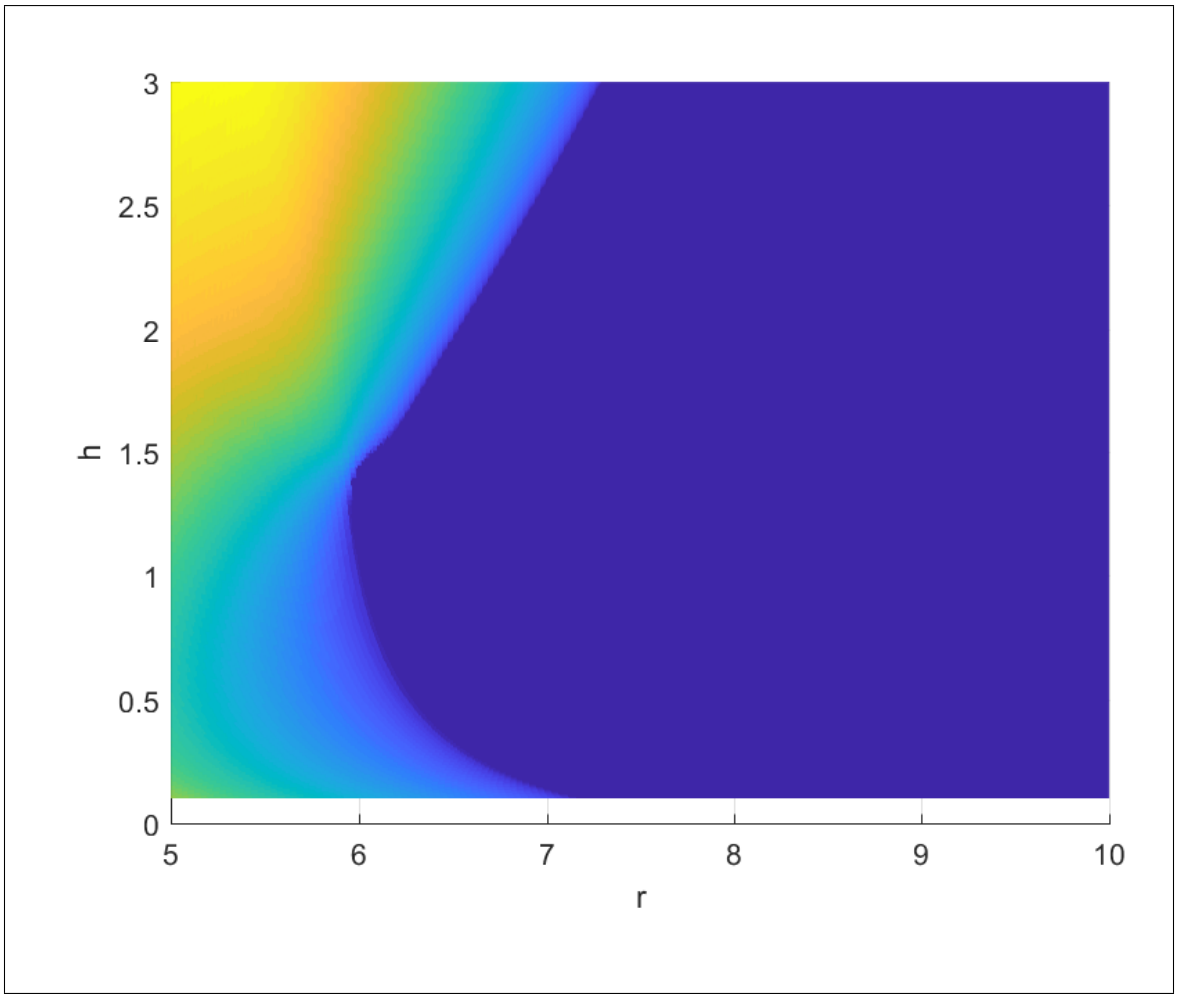

Figure 3.9:

3.4 Phase III

The objective of Phase III is to demonstrate the optimized gradient vector field guidance presented in Phase II on multirotor UAV flying with fixed wing turn-rate constraints.

3.5 Summary of Methodology

4 Results

4.1 Introduction to Results

4.2 Phase I

How quickly the UAV converges and follows the path is determined by the combination of convergence and circulation weights. A low circulation weight allows convergence to dominate the guidance, causing the UAV to quickly reach the path, however will have significant overshoot and may continue to oscillate. High convergence weights prevent oscillation but increase the time taken to converge to the path. Multiple UAV routes for a UAV traveling at a speed of $u = 20m/s$ using guidance of various path circulation weights and convergence $G = 1$ is shown in Figure 4.1 below. The lateral error from the path is shown in Figure 4.2.

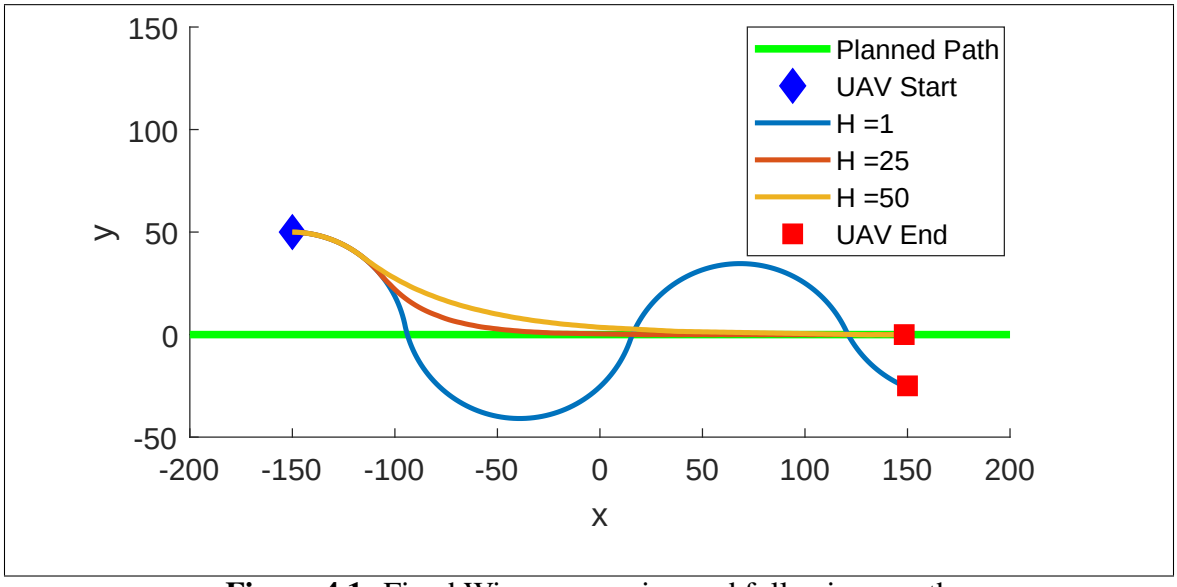

Figure 4.1: Fixed Wing converging and following a path

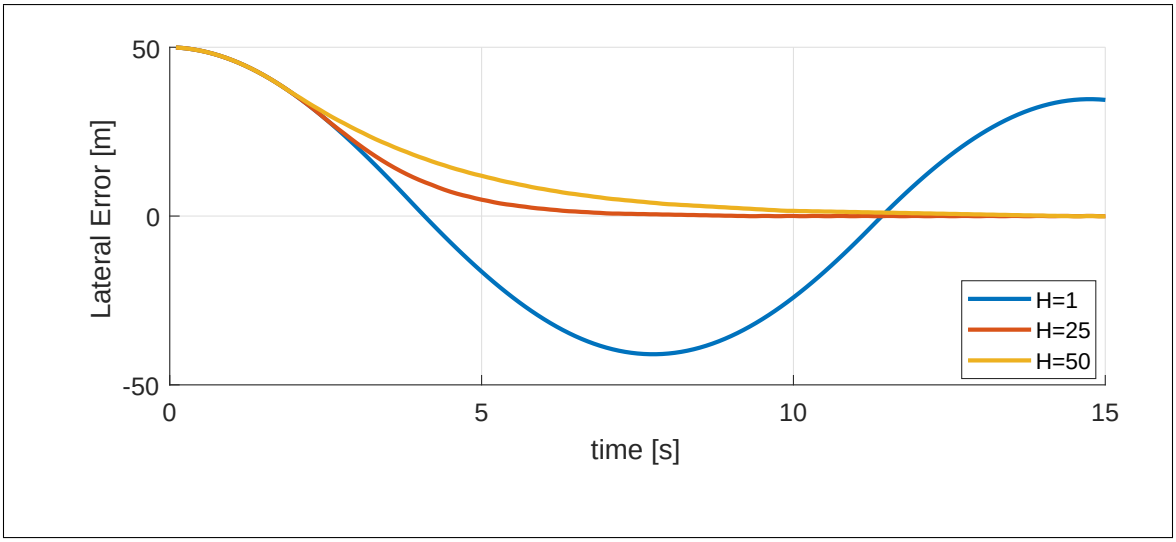

Figure 4.2: Fixed Wing converging and following a path

Guidance for a path at angle $\delta = 0$ and equal parts circulation and convergence weights $G = H = 1$ is shown in Figure 4.3a. How quickly the path following field transitions from convergence to circulation depends on the field weights. Equal parts convergence and circulation are shown in Figure 4.3a ($G = H = 1$) and a larger circulation value in Figure 4.3b ($G = 1, H = 5$).

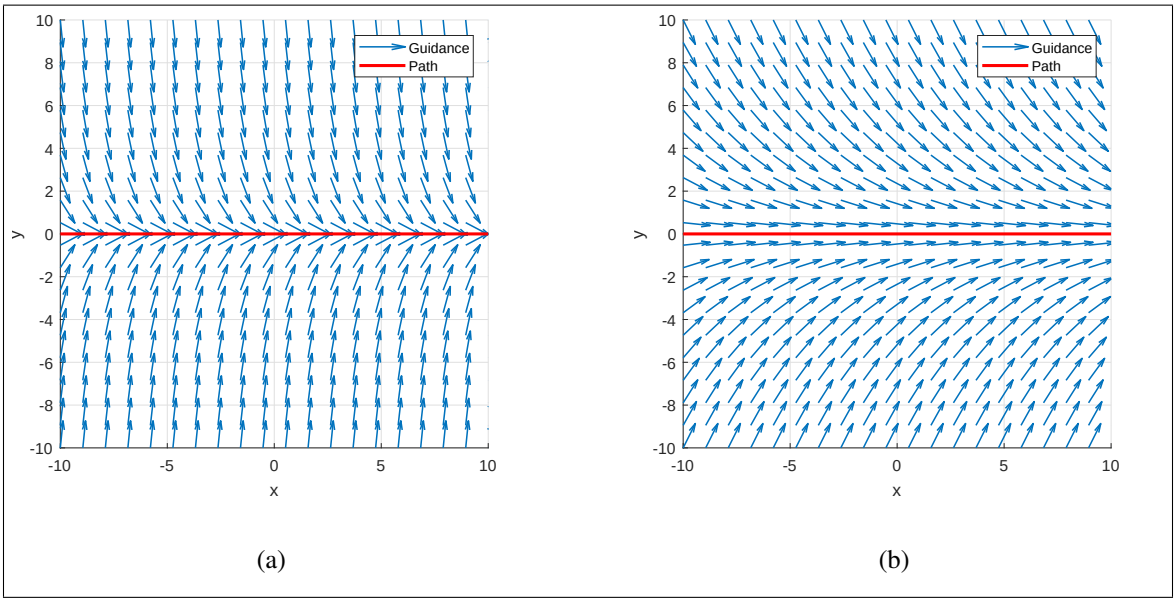

Figure 4.3: GVF converging and a) small circulation b) large circulation

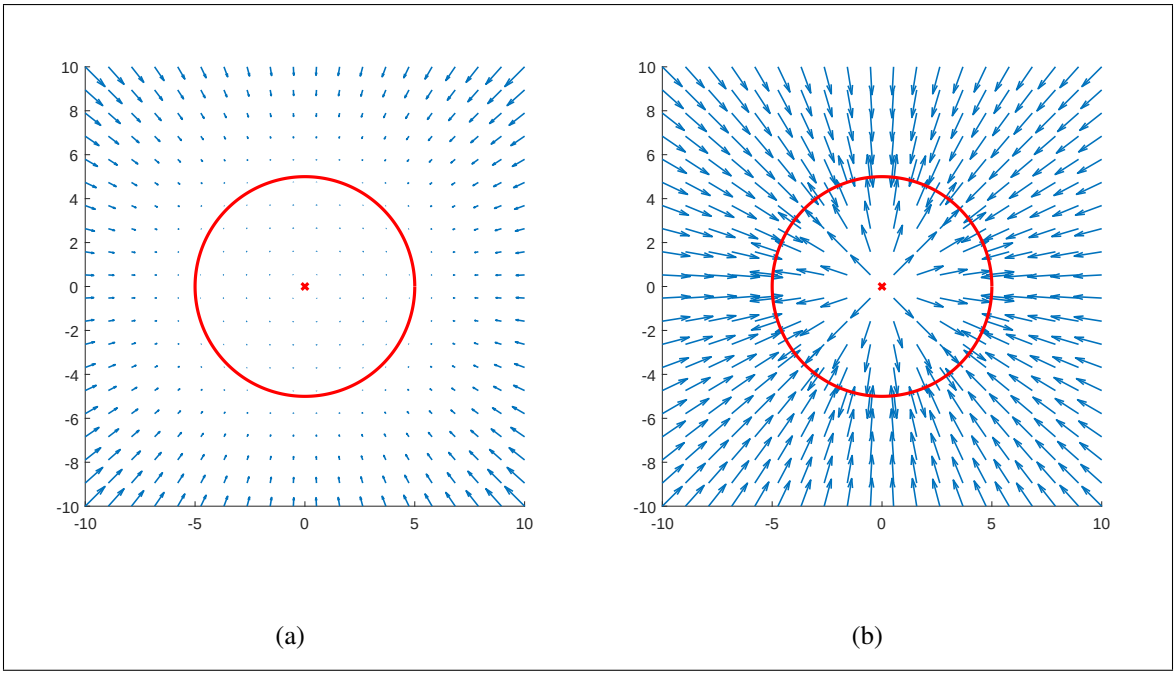

Figure 4.4: GVF circular attractive field without normalization (a) and normalization (b)

Guidance that repels from a circular path can be produced by setting the convergence weight $G = -1$, shown in Figure 4.5.

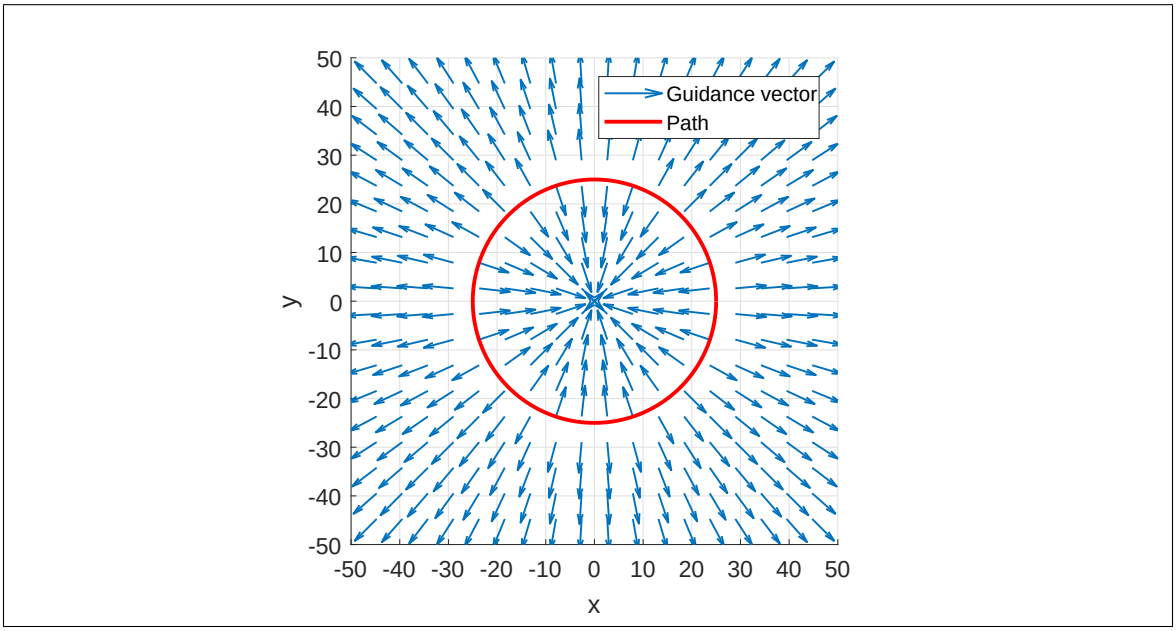

Figure 4.5: Repulsive Circular Field with Large Radius

Note that inside of the path, vectors point towards the center of the circle which may produce a trap situation if the UAV ends up inside the radius. The radius of the path can be reduced, as shown in Figure 4.6 where $r = 0.01$, to prevent trap situations.

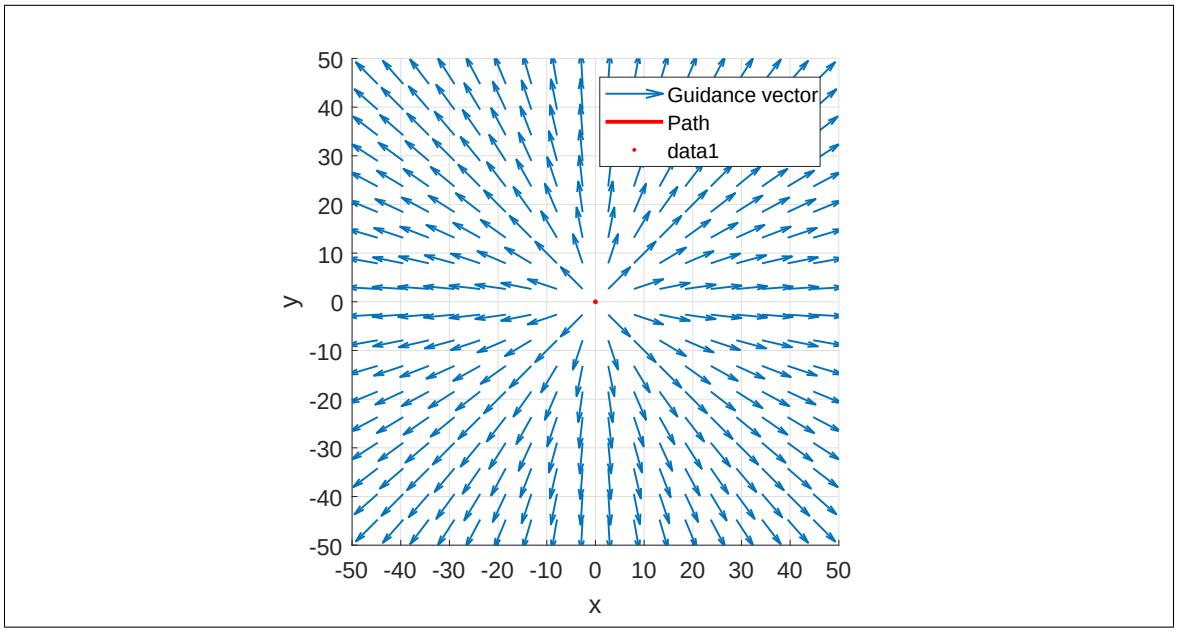

Figure 4.6: Repulsive Circular Field with Small Radius

Evaluating the circulation term results in a vector field that is parallel to a circular path, shown in Figure 4.7a. The field is normalized to produce a field with equal length vectors for the configuration space which is shown in Figure 4.7b.

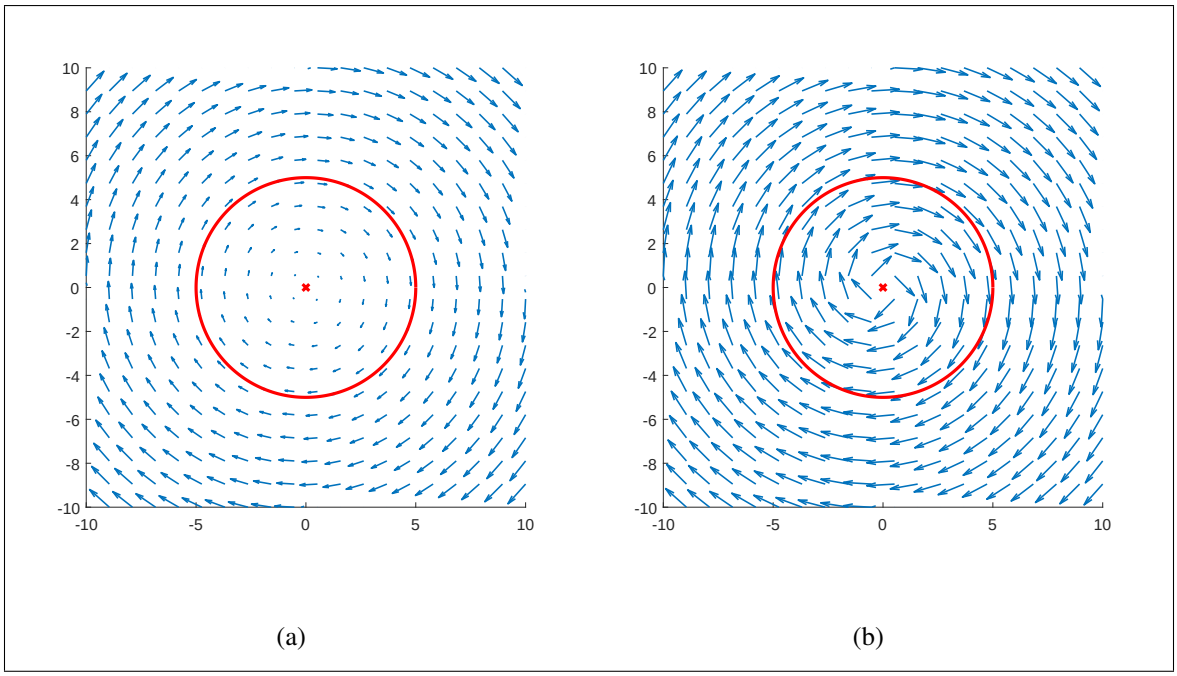

Figure 4.7: Circular GVF without normalization (a) and with normalization (b)

A strictly repulsive field $\overrightarrow{V}_{obst}$ with $G = -1$, $H = 0$, $r = 0.01$, and $R = 35$ is shown in Figure 4.8a. Adding equal magnitude circulation and decay $G = -1$, $H = 1$ is shown in Figure 4.8b.

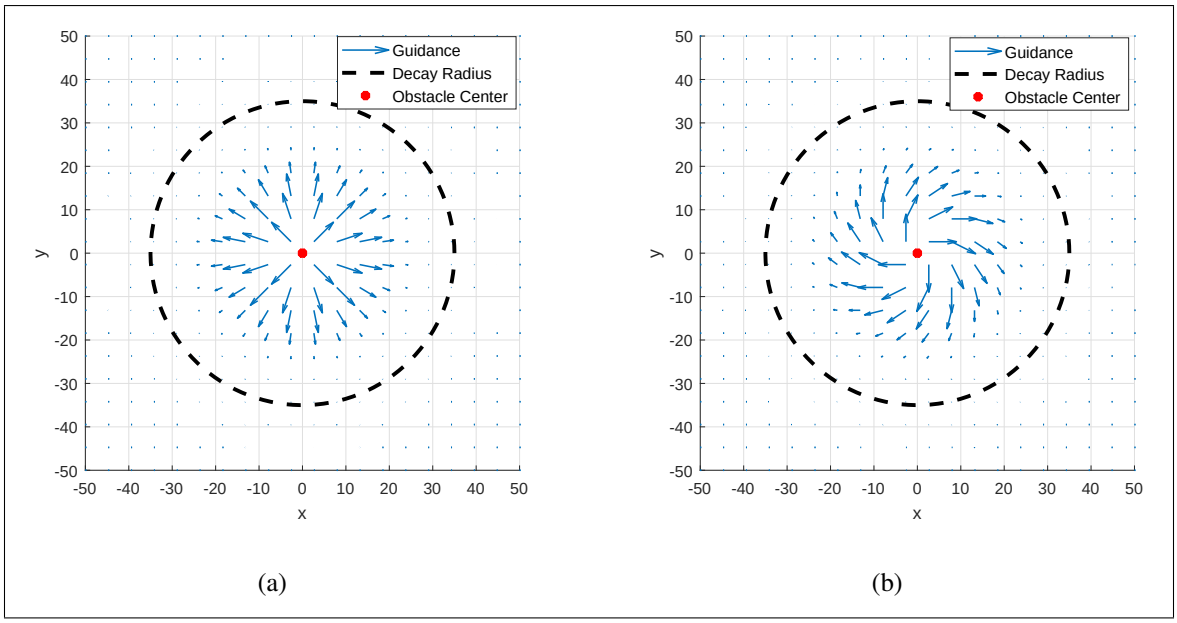

Figure 4.8: Repulsive GVF a) no circulation and b) with circulation

Path following guidance and repulsive obstacle avoidance is achieved by summing the two fields together, producing the UAVs guidance $\overrightarrow{V}_G$ shown in Equation 4.1

$$\overrightarrow{V}_g = \overrightarrow{V}_{path} + P\overrightarrow{V}_{obst} \tag{4.1}$$

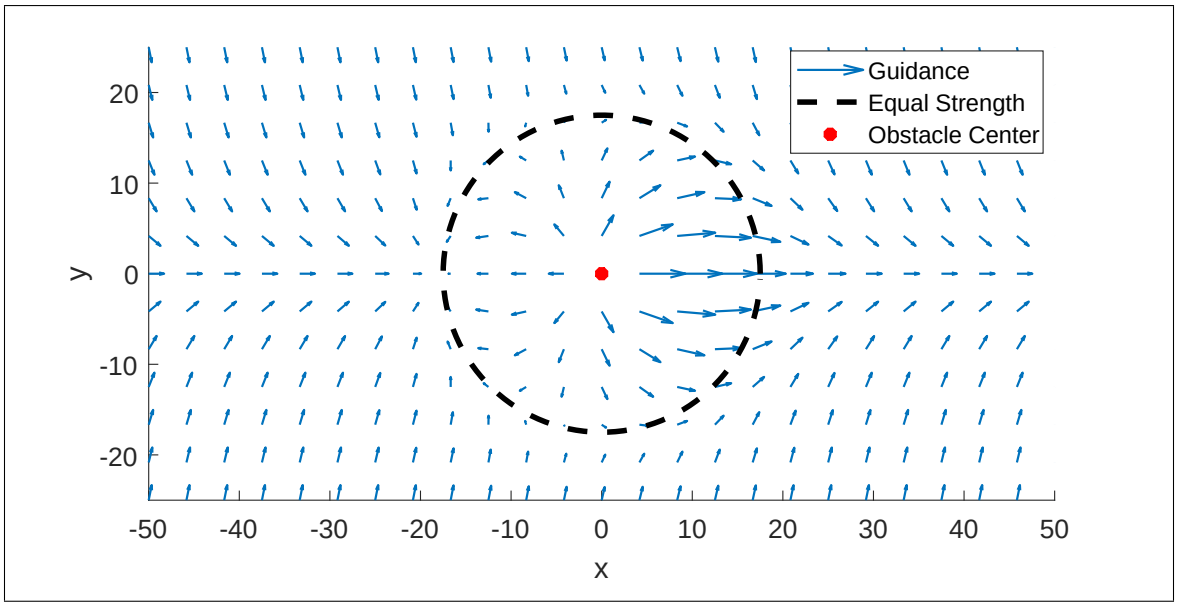

Figure 4.9: Summed Fields Without Total Normalization

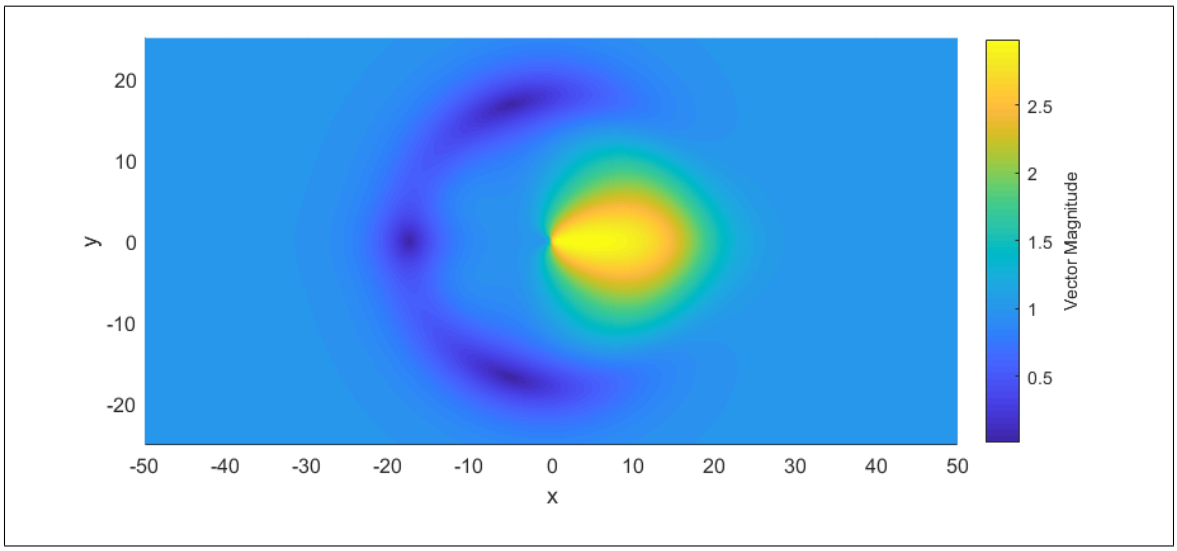

Figure 4.10: Summed Fields Without Total Normalization

Multiple singularities may exist so several initial conditions must be evaluated to detect all singularities present. Several initial conditions placed near the radius of equal strength, $R/2$, on the side of the obstacle where singularities are expected results in the detection of three singularities, shown in Figure 3.6

Evaluating initial conditions both inside and outside of the obstacle radius results in singularity detection. Singularities are a result of two vector fields directly and equally opposing each other, which may be mitigated by modifying the repulsive field with circulation. Equal magnitudes repulsion and circulation $G = -1, H = 1$ are shown in Figure 4.11, which results in a single singularity removed from the planned path as well as the integral guidance line.

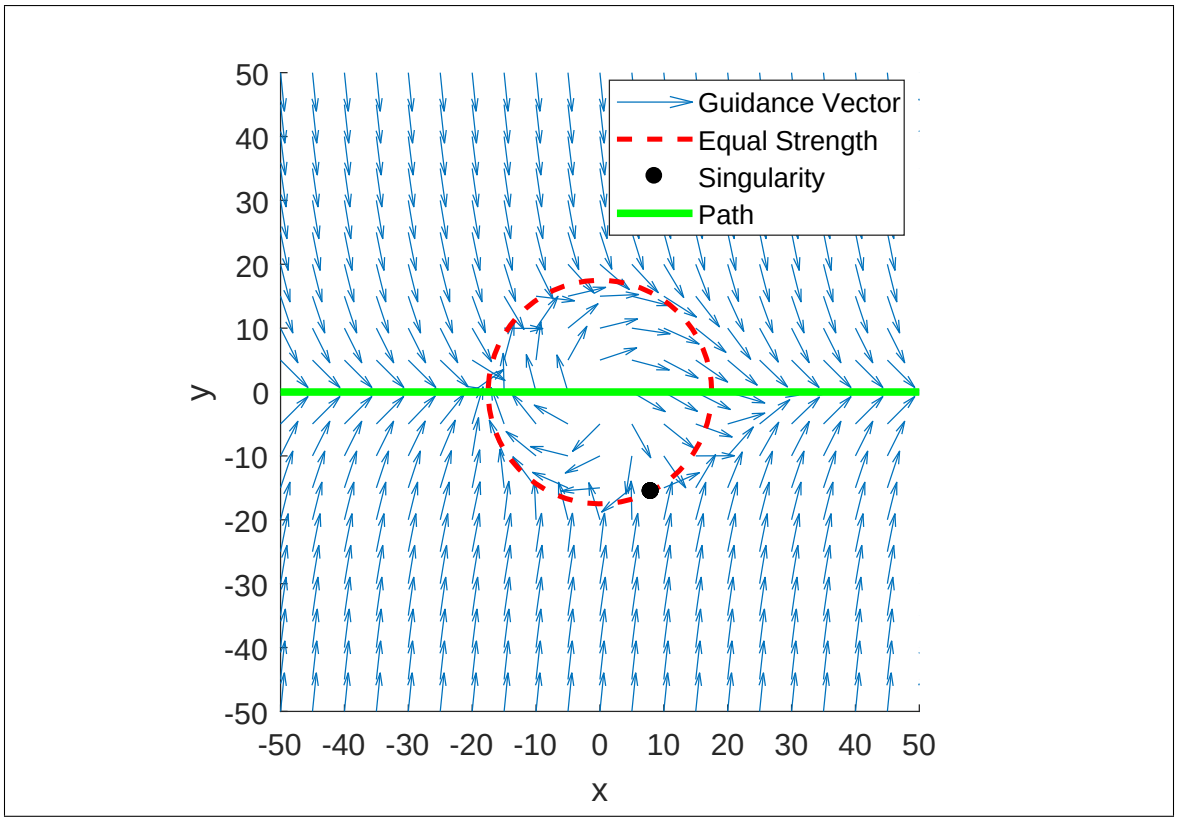

Figure 4.11: Summed Field Guidance with circulation

4.3 Phase II

4.4 Phase III

5 Conclusions

- Singularity detection may also be useful when summing wind fields into guidance
- Expand optimized GVF weights for a curved planned path
- (not future work, general thought: Justification for fixed wings -¿ multirotors can stop, modify altitude, and continue along path to prevent collisions. fixed wings must maintain forward velocity, therefore some type of turning avoidance action is required)

6 Future Work

REFERENCES

[1] Bone, E., "UAVs backbround and issues for congress.pdf," 2003.

[2] Panagou, D., "Motion planning and collision avoidance using navigation vector fields," *Robotics and Automation (ICRA), 2014 IEEE International Conference on*, IEEE, 2014, pp. 2513–2518.

[3] Ariyur, K. B. and Fregene, K. O., "Autonomous tracking of a ground vehicle by a UAV," *American Control Conference, 2008*, IEEE, 2008, pp. 669–671.

[4] Teuliere, C., Eck, L., and Marchand, E., "Chasing a moving target from a flying UAV," *Intelligent Robots and Systems (IROS), 2011 IEEE/RSJ International Conference on*, IEEE, 2011, pp. 4929–4934.

[5] Oh, H., Kim, S., Shin, H.-S., Tsourdos, A., and White, B., "Coordinated standoff tracking of groups of moving targets using multiple UAVs," *Control & Automation (MED), 2013 21st Mediterranean Conference on*, IEEE, 2013, pp. 969–977.

[6] Hyondong Oh, Seungkeun Kim, Hyo-sang Shin, and Tsourdos, A., "Coordinated standoff tracking of moving target groups using multiple UAVs," *IEEE Transactions on Aerospace and Electronic Systems*, Vol. 51, No. 2, April 2015, pp. 1501–1514.

[7] Ulun, S. and Unel, M., "Coordinated motion of UGVs and a UAV," *Industrial Electronics Society, IECON 2013-39th Annual Conference of the IEEE*, IEEE, 2013, pp. 4079–4084.

[8] Beard, R. W. and McLain, T. W., *Small unmanned aircraft: theory and practice*, Princeton University Press, Princeton, N.J, 2012, OCLC: ocn724663112.

[9] Sujit, P., Saripalli, S., and Sousa, J. B., "Unmanned Aerial Vehicle Path Following: A Survey and Analysis of Algorithms for Fixed-Wing Unmanned Aerial Vehicless," *IEEE Control Systems*, Vol. 34, No. 1, Feb. 2014, pp. 42–59.

[10] Khatib, O., "Real-time obstacle avoidance for manipulators and mobile robots," *The international journal of robotics research*, Vol. 5, No. 1, 1986, pp. 90–98.

[11] Rimon, E., "Exact Robot Navigation Using Artificial Potential Functions.pdf," 1992.

[12] Liu, Y. and Zhao, Y., "A virtual-waypoint based artificial potential field method for UAV path planning," *Guidance, Navigation and Control Conference (CGNCC), 2016 IEEE Chinese*, IEEE, 2016, pp. 949–953.

[13] Borenstein, J. and Koren, Y., "Real-time obstacle avoidance for fast mobile robots in cluttered environments," *Robotics and Automation, 1990. Proceedings., 1990 IEEE International Conference on*, IEEE, 1990, pp. 572–577.

[14] Borenstein, J. and Koren, Y., "The vector field histogram-fast obstacle avoidance for mobile robots," *IEEE transactions on robotics and automation*, Vol. 7, No. 3, 1991, pp. 278–288.

[15] Koren, Y. and Borenstein, J., "Potential Field Methods and their inherent limitions for morbile robot navigation.pdf," 1991.

[16] Kim, D. H., "Escaping route method for a trap situation in local path planning," *International Journal of Control, Automation and Systems*, Vol. 7, No. 3, June 2009, pp. 495–500.

[17] Goerzen, C., Kong, Z., and Mettler, B., "A Survey of Motion Planning Algorithms from the Perspective of Autonomous UAV Guidance," *Journal of Intelligent and Robotic Systems*, Vol. 57, No. 1-4, Jan. 2010, pp. 65–100.

[18] Lei Tang, Songyi Dian, Gangxu Gu, Kunli Zhou, Suihe Wang, and Xinghuan Feng, "A novel potential field method for obstacle avoidance and path planning of mobile robot," IEEE, July 2010, pp. 633–637.

[19] Li, G., Yamashita, A., Asama, H., and Tamura, Y., "An efficient improved artificial potential field based regression search method for robot path planning," IEEE, Aug. 2012, pp. 1227–1232.

[20] Nelson, D. R., "Cooperative control of miniature air vehicles," 2005.

[21] Nelson, D. R., Barber, D. B., McLain, T. W., and Beard, R. W., "Vector field path following for small unmanned air vehicles," *American Control Conference, 2006*, IEEE, 2006, pp. 7–pp.

[22] Nelson, D., Barber, D., McLain, T., and Beard, R., "Vector Field Path Following for Miniature Air Vehicles," *IEEE Transactions on Robotics*, Vol. 23, No. 3, June 2007, pp. 519–529.

[23] Jung, W., Lim, S., Lee, D., and Bang, H., "Unmanned Aircraft Vector Field Path Following with Arrival Angle Control," *Journal of Intelligent & Robotic Systems*, Vol. 84, No. 1-4, Dec. 2016, pp. 311–325.

[24] Griffiths, S., "Vector Field Approach for Curved Path Following for Miniature Aerial Vehicles," American Institute of Aeronautics and Astronautics, Aug. 2006.

[25] Frew, E., "Lyapunov Guidance Vector Fields for Unmanned Aircraft Applications.pdf," .

[26] Frew, E. W., "Cooperative standoff tracking of uncertain moving targets using active robot networks," *Robotics and Automation, 2007 IEEE International Conference on*, IEEE, 2007, pp. 3277–3282.

[27] Chen, H., Chang, K., and Agate, C. S., "Tracking with UAV using tangent-plus-Lyapunov vector field guidance," *Information Fusion, 2009. FUSION'09. 12th International Conference on*, IEEE, 2009, pp. 363–372.

[28] Chen, H., Chang, K., and Agate, C. S., "UAV path planning with tangent-plus-Lyapunov vector field guidance and obstacle avoidance," *IEEE Transactions on Aerospace and Electronic Systems*, Vol. 49, No. 2, 2013, pp. 840–856.

[29] Liang, Y. and Jia, Y., "Tangent vector field approach for curved path following with input saturation," *Systems & Control Letters*, Vol. 104, June 2017, pp. 49–58.

[30] Pereira, G. A. S., Choudhury, S., and Scherer, S., "A framework for optimal repairing of vector field-based motion plans," IEEE, June 2016, pp. 261–266.

[31] Pimenta, L. C., Pereira, G. A., and Mesquita, R. C., "Fully continuous vector fields for mobile robot navigation on sequences of discrete triangular regions," *Robotics and Automation, 2007 IEEE International Conference on*, IEEE, 2007, pp. 1992–1997.

[32] Md, Z., Rg, C., and Dj, G., "Simplex Solutions for Optimal Control Flight Paths in Urban Environments," *Journal of Aeronautics & Aerospace Engineering*, Vol. 06, No. 03, 2017.

[33] Zhou, D. and Schwager, M., "Vector field following for quadrotors using differential flatness," IEEE, May 2014, pp. 6567–6572.

[34] Goncalves, V. M., Pimenta, L. C. A., Maia, C. A., and Pereira, G. A. S., "Artificial vector fields for robot convergence and circulation of time-varying curves in n-dimensional spaces," IEEE, 2009, pp. 2012–2017.

[35] Gonçalves, V. M., Pimenta, L. C., Maia, C. A., Pereira, G. A., Dutra, B. C., Michael, N., Fink, J., and Kumar, V., "Circulation of curves using vector fields: actual robot experiments in 2D and 3D workspaces," *Robotics and Automation (ICRA), 2010 IEEE International Conference on*, IEEE, 2010, pp. 1136–1141.

[36] Gonçalves, V. M., Pimenta, L. C., Maia, C. A., Dutra, B. C., and Pereira, G. A., "Vector fields for robot navigation along time-varying curves in $ n $-dimensions," *IEEE Transactions on Robotics*, Vol. 26, No. 4, 2010, pp. 647–659.

[37] Gerlach, A. R., *Autonomous Path-Following by Approximate Inverse Dynamics and Vector Field Prediction*, University of Cincinnati, 2014.